Precision Engineering 79 (2023) 60–77

Contents lists available at ScienceDirect

Precision Engineering

journal homepage: www.elsevier.com/locate/precision

Review and status of tool tip frequency response function prediction using receptance coupling☆

Tony Schmitz [a,b,*], Emma Betters [a,b], Erhan Budak [c], Esra Yüksel [c], Simon Park [d], Yusuf Altintas [e]

[a] Mechanical, Aerospace, and Biomedical Engineering, University of Tennessee, Knoxville, Knoxville, TN, USA
[b] Manufacturing Science Division, Oak Ridge National Laboratory, Oak Ridge, TN, USA
[c] Manufacturing Research Laboratory, Sabanci University, Istanbul, Turkey
[d] Mechanical and Manufacturing Engineering, University of Calgary, Calgary, Alberta, Canada
[e] Mechanical Engineering, University of British Columbia, Vancouver, BC, Canada

ARTICLE INFO

Keywords:
Machining
Milling
Dynamics
Receptance coupling
Frequency response function

ABSTRACT

This paper provides a chronological review of publications that implement and advance the receptance coupling substructure analysis (RCSA) approach first applied to tool tip receptance (or frequency response function) prediction for milling applications in 2000. The review topics mimic the RCSA approach, where the tool, holder, and spindle-machine receptances are coupled analytically, and include: tool-holder receptance modeling; connection modeling; spindle-machine receptances; and applications. The review paper summarizes contributions from multiple, international authors (198 papers) to these topics. It also provides a comprehensive resource for those beginning an investigation into RCSA.

1. Introduction

Receptance coupling is a technique where component/substructure receptances, or frequency response functions (FRFs), are joined analytically to predict assembly dynamics. It was first introduced in 1960 by Bishop and Johnson [1] and has become a standard approach in structural dynamics modeling over the past decades. In 2000, Schmitz and Donaldson [2] applied receptance coupling substructure analysis (RCSA) for the first time to tool tip receptance prediction for tool-holder-spindle-machine assemblies used in milling applications. In the following 20+ years, numerous authors have implemented and improved the approach. Fig. 1 displays the number of RCSA-related publications from 2000 to March 2022. Topics of investigation have included, for example:

- modeling the tool and holder using analytical and numerical solutions
- describing the non-rigid, damped connection between the tool and holder and holder and spindle
- identifying the spindle-machine receptances by measurement and modeling
- mathematical frameworks for completing RCSA predictions of assembly dynamics from component receptances
- application to milling stability prediction.

The key advantages of the RCSA approach are:

- provides an analytical prediction of the tool tip FRF
- enables models and measurements of assembly components to be coupled
- may include all measured or modeled vibration modes within the desired bandwidth without computational penalty.

These are discussed in greater detail in the review paper, which summarizes prior research studies and provides a comprehensive

☆ This work was supported by the DOE Office of Energy Efficiency and Renewable Energy (EERE), Advanced Manufacturing Office (AMO), under contract DE-AC05-00OR22725. The US government retains and the publisher, by accepting the article for publication, acknowledges that the US government retains a nonexclusive, paid-up, irrevocable, worldwide license to publish or reproduce the published form of this manuscript, or allow others to do so, for US government purposes. DOE will provide public access to these results of federally sponsored research in accordance with the DOE Public Access Plan (http://energy.gov/downloads/doe-public-access-plan).

* Corresponding author. Mechanical, Aerospace, and Biomedical Engineering, University of Tennessee, Knoxville, Knoxville, TN, USA..
E-mail address: tony.schmitz@utk.edu (T. Schmitz).

https://doi.org/10.1016/j.precisioneng.2022.09.008
Received 6 July 2022; Received in revised form 24 September 2022; Accepted 27 September 2022
Available online 1 October 2022
0141-6359/© 2022 Elsevier Inc. All rights reserved.

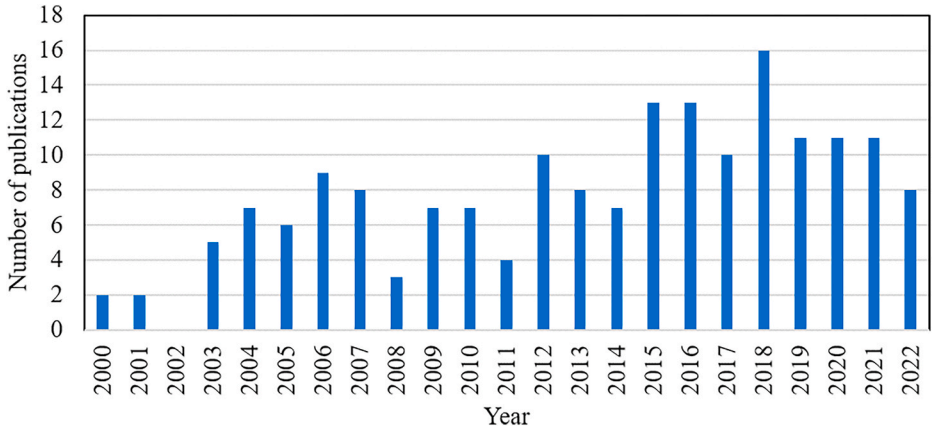

Fig. 1. Number of RCSA-related publications per year (2000 to March 2022).

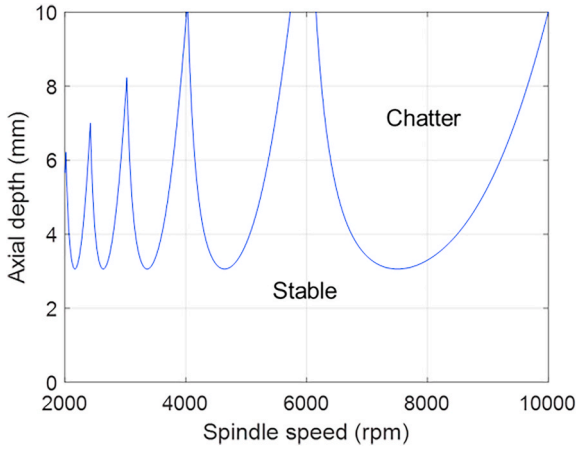

Fig. 2. Stability map for milling performance prediction. The map separates stable and unstable (chatter) combinations of spindle speed and axial depth of cut for a selected radial depth of cut.

resource for those beginning an investigation on this topic. The paper concludes by describing remaining opportunities to address remaining research and application gaps.

The paper is organized as follows. A description of the RCSA algorithm is first presented to provide context and vocabulary for the remaining sections. In these following sections, the research efforts are grouped based on the RCSA modeling approach: Tool-holder receptance modeling (in this paper, tool is used to denote the cutting tool, holder is used to denote the tool holder, and tool-holder indicates the combination of the tool and tool holder); Connection modeling; Spindle-machine receptances; and Applications. In each section, contributions are ordered by year of publication to demonstrate the sequence of research discoveries and efforts. Conclusions are finally presented to complete the review and identify remaining knowledge gaps.

2. RCSA description

The original intent of RCSA was to reduce the number of tool tip FRF measurements required in production environments. Because the tool tip FRF is a key input to milling stability analyses that separate stable and unstable (chatter) combinations of spindle speed and axial depth of cut, a measurement is typically required for each tool-holder-spindle-machine combination [3–6]. For manufacturing facilities with many machines or limited FRF measurement resources, this poses a significant obstacle to the implementation of stability maps for optimized parameter selection; see Fig. 2. By enabling prediction of the tool tip dynamics

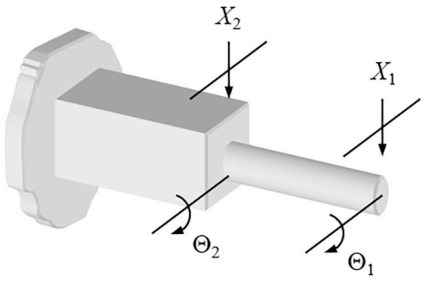

Fig. 3. RCSA example for a cylinder rigidly coupled to a prismatic cantilever beam to form an assembly.

from a limited set of information, the number of required tool tip FRF measurements can be dramatically reduced.

There are three key advantages of the RCSA approach over the more traditional finite element modeling approach used in machine tool design. First, RCSA provides an analytical, closed-form prediction of the tool tip FRF so it is computationally efficient. This enables a large parameter space to be studied quickly (e.g., variation in tool tip FRF with changes in the tool extension length from the holder). Second, RCSA enables models and measurements to be seamlessly combined in the frequency domain analysis. Those components with relatively simple geometries and few connections, such as the tool and holder, are described using standard analytical or numerical modeling approaches, including Euler-Bernoulli or Timoshenko beam models. Components that are not convenient to model, such as direct drive milling spindles with proprietary geometries and unknown bearing stiffness values, are measured and archived. The model-measurement combination is particularly relevant when assembly measurements are challenging, such as tool tip FRF identification for micro-endmills. In this case, the micro-endmills may be conveniently modeled, but it may not be possible to provide a tool tip impact test due to the endmill size. Third, because the RCSA vector calculations are performed in the frequency domain, there is no computational penalty for including all measured or modeled vibration modes within the desired frequency range.

In the following paragraphs, key elements of the RCSA procedure are detailed to provide a basis for a review of the research efforts that have followed the initial study [2]. The RCSA model includes: 1) transverse deflections, x_i and X_i, for the components (lower case variables) and assembly (upper case variables) due to internal and external forces, f_j and F_j; and 2) rotations about lines perpendicular to the beam axis, θ_i and Θ_i, and bending moments (or couples), m_j and M_j, to completely describe the transverse dynamic behavior of beams. To describe the procedure, consider the cylinder-prismatic cantilever beam assembly displayed in Fig. 3. This is representative of a tool (cylinder) rigidly

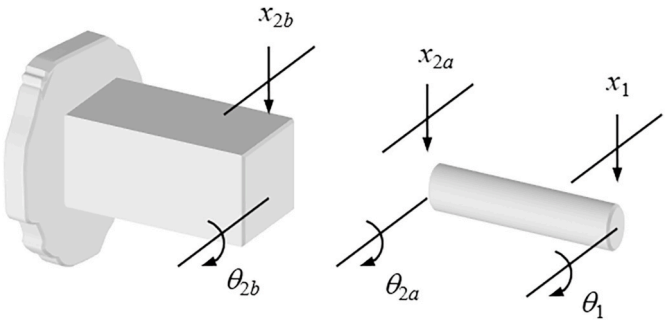

Fig. 4. Cylinder and prismatic cantilever beam components for RCSA example.

attached to a holder-spindle-machine (prismatic cantilever beam).

To calculate the assembly receptances, all four bending receptances are included in the component (i.e., cylinder and prismatic cantilever beam) descriptions. These four bending receptances include displacement-to-force, h_{ij}, displacement-to-couple, l_{ij}, rotation-to-force, n_{ij}, and rotation-to-couple, p_{ij}, where i is the displacement/rotation coordinate location and j is the location where the force/couple is applied. There are three primary steps followed to predict Fig. 3 assembly receptances.

1. Define the components and coordinates for the model. In this example, there are two components: a prismatic beam with fixed-free (or cantilever) boundary conditions and a cylinder with free-free (or unsupported) boundary conditions; see Fig. 4.
2. Determine the component receptances. These can be based on measurements or models. For the models, an analytical choice is closed-form receptances for flexural vibrations of uniform Euler-Bernoulli beams with free, fixed, sliding, and pinned boundary conditions [1,7]. A numerical option is the Timoshenko beam model [8]. In either case, the fluted section of the endmill must be accurately represented. This may be completed using an equivalent diameter cylinder or a full finite element model with the actual flute geometry; see Section 4. For measurements, tap testing may be applied, where the structure is excited using a modal hammer (impact force) or shaker-stinger combination (sinusoidal, chirp, or other force profile) and the response is measured using a linear transducer, such as a low-mass accelerometer [7].
3. Based on the model from step 1, express the assembly receptances as a function of the component receptances from step 2. Determine the assembly receptances using the component displacements/rotations, compatibility conditions, and equilibrium conditions.

The procedure for coupling the components in Fig. 4 to form the assembly in Fig. 3 requires the component receptances. In Fig. 4, coordinates are placed at the prediction location (1) and coupling locations (2a and 2b) on the two components. For the cylinder, the direct receptances at the coordinate 1 end are shown in Eq. (1).

$$h_{11}=\frac{x_1}{f_1}\,l_{11}=\frac{x_1}{m_1}\,n_{11}=\frac{\theta_1}{f_1}\,p_{11}=\frac{\theta_1}{m_1} \tag{1}$$

The cross receptances are given by Eq. (2).

$$h_{12a}=\frac{x_1}{f_{2a}}\,l_{12a}=\frac{x_1}{m_{2a}}\,n_{12a}=\frac{\theta_1}{f_{2a}}\,p_{12a}=\frac{\theta_1}{m_{2a}} \tag{2}$$

At coordinate 2a on the cylinder, the direct and cross receptances are provided in Eqs. (3) and (4).

$$h_{2a2a}=\frac{x_{2a}}{f_{2a}}\,l_{2a2a}=\frac{x_{2a}}{m_{2a}}\,n_{2a2a}=\frac{\theta_{2a}}{f_{2a}}\,p_{2a2a}=\frac{\theta_{2a}}{m_{2a}} \tag{3}$$

$$h_{2a1}=\frac{x_{2a}}{f_1}\,l_{2a1}=\frac{x_{2a}}{m_1}\,n_{2a1}=\frac{\theta_{2a}}{f_1}\,p_{2a1}=\frac{\theta_{2a}}{m_1} \tag{4}$$

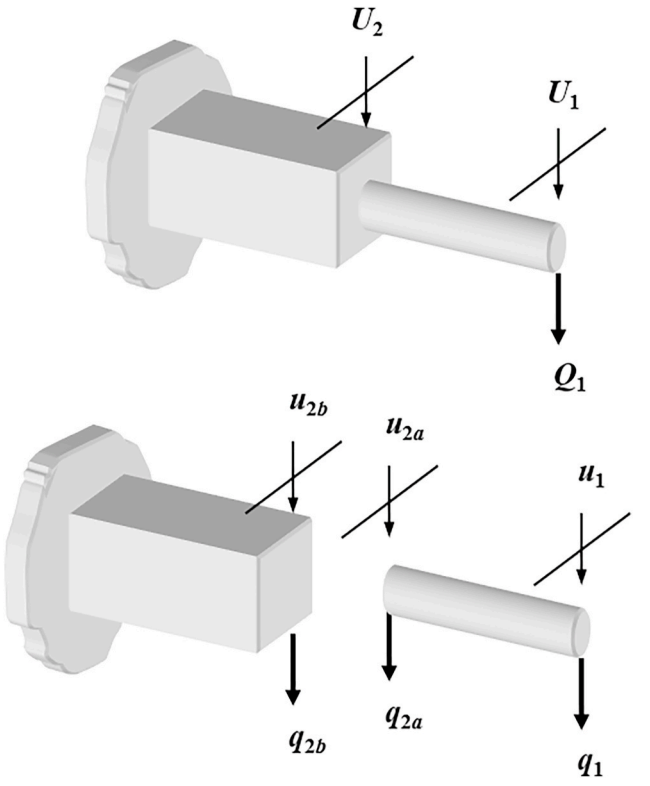

Fig. 5. Receptance coupling model for determining $\boldsymbol{G_{11}}$ using a rigid connection. (Top) assembly. (Bottom) components.

Similarly, for the prismatic cantilever beam, the direct receptances at the coupling location 2b are given by Eq. (5).

$$h_{2b2b}=\frac{x_{2b}}{f_{2b}}\,l_{2b2b}=\frac{x_{2b}}{m_{2b}}\,n_{2b2b}=\frac{\theta_{2b}}{f_{2b}}\,p_{2b2b}=\frac{\theta_{2b}}{m_{2b}} \tag{5}$$

To simplify notation, the component receptances may be represented in matrix form as shown in Eq. 6 through 9 for the cylinder and Eq. (10) for the prismatic cantilever beam. In Eqs. (6)–(10) R_{ij} is the generalized receptance matrix that describes both translational and rotational component behavior [9] and u_i and q_j are the corresponding generalized displacement/rotation and force/couple vectors.

$$\begin{Bmatrix} x_1 \\ \theta_1 \end{Bmatrix}=\begin{bmatrix} h_{11} & l_{11} \\ n_{11} & p_{11} \end{bmatrix}\begin{Bmatrix} f_1 \\ m_1 \end{Bmatrix}\text{or } \{\boldsymbol{u_1}\}=[\boldsymbol{R_{11}}]\{\boldsymbol{q_1}\} \tag{6}$$

$$\begin{Bmatrix} x_{2a} \\ \theta_{2a} \end{Bmatrix}=\begin{bmatrix} h_{2a2a} & l_{2a2a} \\ n_{2a2a} & p_{2a2a} \end{bmatrix}\begin{Bmatrix} f_{2a} \\ m_{2a} \end{Bmatrix}\text{or } \{\boldsymbol{u_{2a}}\}=[\boldsymbol{R_{2a2a}}]\{\boldsymbol{q_{2a}}\} \tag{7}$$

$$\begin{Bmatrix} x_1 \\ \theta_1 \end{Bmatrix}=\begin{bmatrix} h_{12a} & l_{12a} \\ n_{12a} & p_{12a} \end{bmatrix}\begin{Bmatrix} f_{2a} \\ m_{2a} \end{Bmatrix}\text{or } \{\boldsymbol{u_1}\}=[\boldsymbol{R_{12a}}]\{\boldsymbol{q_{2a}}\} \tag{8}$$

$$\begin{Bmatrix} x_{2a} \\ \theta_{2a} \end{Bmatrix}=\begin{bmatrix} h_{2a1} & l_{2a1} \\ n_{2a1} & p_{2a1} \end{bmatrix}\begin{Bmatrix} f_1 \\ m_1 \end{Bmatrix}\text{or } \{\boldsymbol{u_{2a}}\}=[\boldsymbol{R_{2a1}}]\{\boldsymbol{q_1}\} \tag{9}$$

$$\begin{Bmatrix} x_{2b} \\ \theta_{2b} \end{Bmatrix}=\begin{bmatrix} h_{2b2b} & l_{2b2b} \\ n_{2b2b} & p_{2b2b} \end{bmatrix}\begin{Bmatrix} f_{2b} \\ m_{2b} \end{Bmatrix}\text{or } \{\boldsymbol{u_{2b}}\}=[\boldsymbol{R_{2b2b}}]\{\boldsymbol{q_{2b}}\} \tag{10}$$

The component receptances are written using the generalized notation: $\boldsymbol{u_1}=\boldsymbol{R_{11}q_1}+\boldsymbol{R_{12a}q_{2a}}$ and $\boldsymbol{u_{2a}}=\boldsymbol{R_{2a1}q_1}+\boldsymbol{R_{2a2a}q_{2a}}$ for the cylinder and $\boldsymbol{u_{2b}}=\boldsymbol{R_{2b2b}q_{2b}}$ for the prismatic cantilever beam. For a rigid connection between the two components, the compatibility condition is $\boldsymbol{u_{2b}}-\boldsymbol{u_{2a}}=0$. This indicates there is no relative motion at the coupling location. Additionally, if the component and assembly coordinates are at the same physical locations, then $\boldsymbol{u_1}=\boldsymbol{U_1}$ and $\boldsymbol{u_{2a}}=\boldsymbol{u_{2b}}=\boldsymbol{U_2}$ (due to the rigid coupling). The assembly receptances are written as shown in Eq. (11),

which again incorporates the generalized notation.

$$\begin{Bmatrix} \boldsymbol{U}_1 \\ \boldsymbol{U}_2 \end{Bmatrix} = \begin{bmatrix} \boldsymbol{G}_{11} & \boldsymbol{G}_{12} \\ \boldsymbol{G}_{21} & \boldsymbol{G}_{22} \end{bmatrix} \begin{Bmatrix} \boldsymbol{Q}_1 \\ \boldsymbol{Q}_2 \end{Bmatrix}, \text{where } \boldsymbol{U}_i = \begin{Bmatrix} X_i \\ \Theta_i \end{Bmatrix}, \boldsymbol{G}_{ij} = \begin{bmatrix} H_{ij} & L_{ij} \\ N_{ij} & P_{ij} \end{bmatrix}, \text{and } \boldsymbol{Q}_j = \begin{Bmatrix} F_j \\ M_j \end{Bmatrix} \tag{11}$$

To determine the four assembly receptances at the free end of the cylinder, $\boldsymbol{G_{11}}$, the generalized force $\boldsymbol{Q_1}$ is applied to assembly coordinate $\boldsymbol{U_1}$ as shown in Fig. 5, where the generalized U_i and u_i vectors are shown schematically as "displacements", although they describe both transverse deflection and rotation. The associated equilibrium conditions are $\boldsymbol{q_{2a}} + \boldsymbol{q_{2b}} = 0$ (i.e., the internal forces/couples are balanced) and $\boldsymbol{q_1} = \boldsymbol{Q_1}$ (because the component and assembly generalized forces are located at the same spatial location).

By substituting the component displacements/rotations and equilibrium conditions into the compatibility condition, the expression for $\boldsymbol{q_{2b}}$ shown in Eq. (12) is obtained. The component force $\boldsymbol{q_{2a}}$ is then determined from the equilibrium condition $\boldsymbol{q_{2a}} = -\boldsymbol{q_{2b}}$.

$$\boldsymbol{u_{2b}} - \boldsymbol{u_{2a}} = 0\ \boldsymbol{R_{2b2b}}\boldsymbol{q_{2b}} - \boldsymbol{R_{2a1}}\boldsymbol{q_1} - \boldsymbol{R_{2a2a}}\boldsymbol{q_{2a}} = 0\ (\boldsymbol{R_{2a2a}} + \boldsymbol{R_{2b2b}})\boldsymbol{q_{2b}} - \boldsymbol{R_{2a1}}\boldsymbol{Q_1} = 0\ \boldsymbol{q_{2b}} = (\boldsymbol{R_{2a2a}} + \boldsymbol{R_{2b2b}})^{-1}\boldsymbol{R_{2a1}}\boldsymbol{Q_1} \tag{12}$$

The expression for $\boldsymbol{G_{11}}$ is given by Eq. (13). The (1, 1) location, H_{11}, in the 2 × 2 matrix, $\boldsymbol{G_{11}}$, is the displacement-to-force receptance required for milling stability prediction.

$$\boldsymbol{G_{11}} = \frac{\boldsymbol{U_1}}{\boldsymbol{Q_1}} = \frac{\boldsymbol{u_1}}{\boldsymbol{Q_1}} = \frac{\boldsymbol{R_{11}}\boldsymbol{q_1} + \boldsymbol{R_{12a}}\boldsymbol{q_{2a}}}{\boldsymbol{Q_1}} = \frac{\boldsymbol{R_{11}}\boldsymbol{Q_1} - \boldsymbol{R_{12a}}(\boldsymbol{R_{2a2a}} + \boldsymbol{R_{2b2b}})^{-1}\boldsymbol{R_{2a1}}\boldsymbol{Q_1}}{\boldsymbol{Q_1}}$$
$$\boldsymbol{G_{11}} = \boldsymbol{R_{11}} - \boldsymbol{R_{12a}}(\boldsymbol{R_{2a2a}} + \boldsymbol{R_{2b2b}})^{-1}\boldsymbol{R_{2a1}} = \begin{bmatrix} H_{11} & L_{11} \\ N_{11} & P_{11} \end{bmatrix} \tag{13}$$

for a non-rigid coupling with energy dissipation (damping) between the tool and holder, Eq. (13) is modified to include a connection stiffness matrix, $[\boldsymbol{K}]$, as shown in Eq. (14).

$$\boldsymbol{G_{11}} = \boldsymbol{R_{11}} - \boldsymbol{R_{12a}}\left(\boldsymbol{R_{2a2a}} + \boldsymbol{R_{2b2b}} + \boldsymbol{K}^{-1}\right)^{-1}\boldsymbol{R_{2a1}} = \begin{bmatrix} H_{11} & L_{11} \\ N_{11} & P_{11} \end{bmatrix} \tag{14}$$

The complex-valued, frequency-dependent connection stiffness matrix is defined in Eq. (15), where k indicates stiffness, c represents viscous damping, and ω is frequency. The subscripts for the 2 × 2 stiffness matrix entries identify their function. For example, $k_{\theta f}$ represents resistance to rotation due to an applied force.

$$[\boldsymbol{K}] = \begin{bmatrix} k_{xf} + i\omega c_{xf} & k_{\theta f} + i\omega c_{\theta f} \\ k_{xm} + i\omega c_{xm} & k_{\theta m} + i\omega c_{\theta m} \end{bmatrix} \tag{15}$$

3. RCSA algorithm

In the initial RCSA study [2], three significant simplifications were applied to predict the tool tip receptances.

- First, the tool was modeled as an Euler-Bernoulli beam. This analytical approximation of transverse bending modes is sufficient for long, slender beams, but loses accuracy for short, non-slender beams [1,7,8].
- Second, the holder-spindle-machine was modeled as a single substructure. While this enables prediction of the effect of changes in tool overhang length, which was the intent of the initial RCSA study [2], the holder-spindle-machine measurement must be repeated for each new holder. This limits the time savings relative to an approach which treats the tool, holder, and spindle-machine as separate substructures (or components).
- Third, due to the difficulty in measuring rotational receptances, the h receptance was measured on the holder-spindle-machine, while the l, n, and p receptances were assumed to be zero.

Despite these simplifications, accurate predictions were presented for a selected holder-spindle-machine substructure and endmill with length-to-diameter ratios of 8:1, 9:1, and 10:1 using a single connection parameter matrix (Eq. (15)); see Fig. 6. Additionally, the corresponding stability maps were presented and the change in critical stability limit was reported for a wide range of overhang lengths. Follow-on papers by Schmitz and colleagues [9–11] expanded the experimental validation using new tool-holder-spindle combinations with the same simplifications.

In 2003, Park et al. [12] extended the RCSA approach to include rotational receptances. One short and one long solid carbide rod were inserted in a tool holder and measured by tap testing; rotational receptances were extracted from direct and cross displacement-to-force measurements. Burns and Schmitz [13] followed this work by incorporating rotational receptances in the holder-spindle-machine model in to study the tool-holder connection parameters.

The next significant step forward in the RCSA approach was to

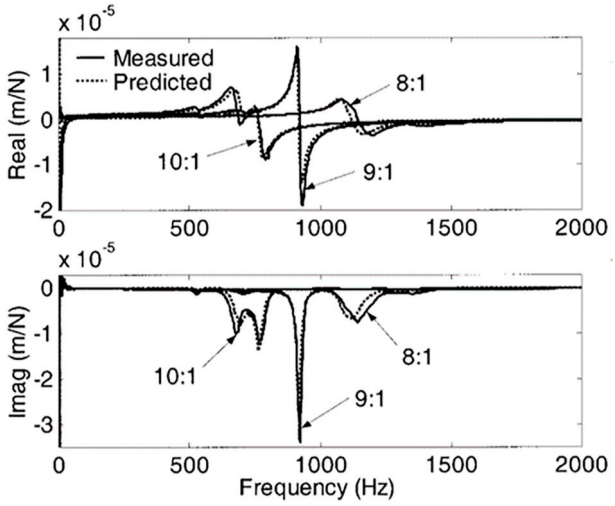

Fig. 6. Predictions and measurements for a selected holder-spindle-machine and endmill with length-to-diameter ratios of 8:1, 9:1, and 10:1. Predictions were completed using a single connection parameter matrix and rigid rotational FRFs for the holder-spindle-machine [2].

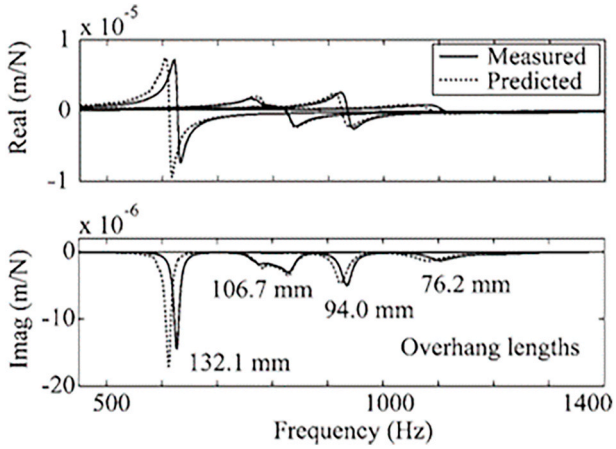

Fig. 7. Tool tip FRF predictions for four different tool extension lengths from a single shrink fit holder-spindle combination. The same connection parameters were used for each prediction [8].

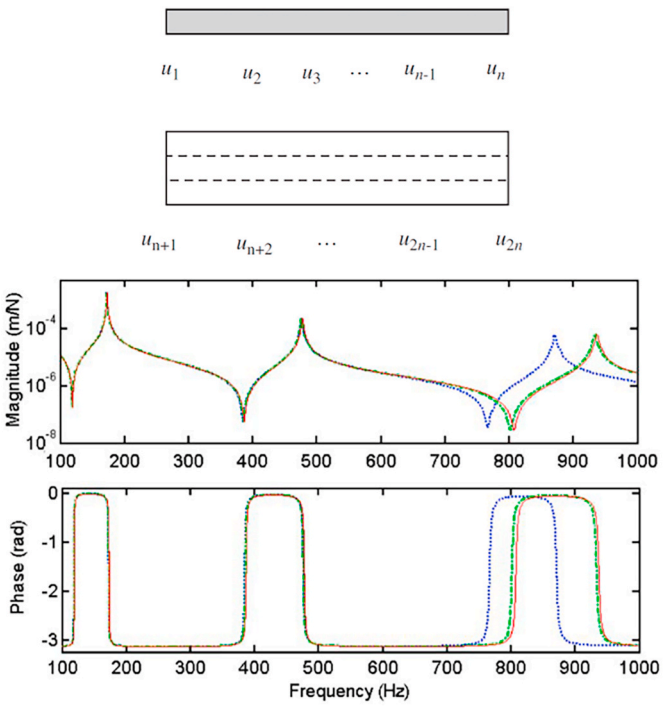

Fig. 8. Nested assembly coupling results for four- and five-point coupling. (Top) Model for n-point coupling. (Bottom) Results for the Euler-Bernoulli composite beam (solid line), $n = 4$ (dotted), and $n = 5$ (dot-dashed) [21].

separate the holder from the spindle-machine to provide a three-component RCSA model: tool, holder, and spindle-machine [14–18]. This provided a more general solution, where the spindle-machine receptances are measured once and archived. Any tool-holder combination can then be modeled and coupled to the archived receptances to predict the tool tip receptance. In the 2005 paper [14], Duncan and Schmitz modeled the tool and holder using both Euler-Bernoulli [1] and Timoshenko beam theory [8] and identified the spindle-machine receptances using a standard artifact. This artifact was a simple geometry holder blank that was inserted in the selected spindle-machine and used to calculate the linear and rotational receptances by direct and cross displacement-to-force measurements. Additional details for these calculations are provided in Section 6. Fig. 7 provides comparisons between measurements and predictions with four different tool extension lengths from a single shrink fit holder-spindle combination. The same connection parameters were used for each prediction. It is seen that an interaction between a spindle mode and the tool-holder mode occurs for the 106.7 mm extension. Schmitz et al. [19,20] described the tool, holder, and spindle-machine as "genes" in the "Machine Tool Genome Project" and used RCSA to predict the assembly FRFs (analogous to physical traits in the human genome) for pre-process parameter selection.

In 2006, Schmitz and Duncan extended the three-component approach to model nested assemblies with coincident neutral axes [21]. Translational and rotational degrees of freedom along the connection between the internal cylindrical tool shank and external cylindrical tool holder were assigned. The approach included any number of connection coordinates with equal and unequal spacing, non-uniform cross-sectional components, and non-rigid contact interfaces. Fig. 8 displays results for four- and five-point coupling of internal and external cylinders with FRFs that include the first three free-free bending modes. It is seen that the five-point coupling solution more accurately represents the third mode; the four-point result aliases the third mode shape.

In 2013, Albertelli et al. [22,23] described an approach to improve the assembly receptance matrix using nine impact measurements to estimate the rotation-to-moment receptance. Wen et al. also modeled three separate substructures: machine-spindle-holder taper, holder-tool shank, and extended portion of the tool. They incorporated the connection parameters as linear and rotational springs and dampers [24]. Hu et al. presented an RCSA method with improved computational efficiency, where an experimental receptance matrix was used to define the spindle-holder joint characteristics [25]. The approach was proposed to more accurately reflect nonlinearities in the system dynamics.

In 2016, Brecher et al. and Montevecchi et al. updated the RCSA algorithm. Brecher et al. detailed an approach for determining the spindle-tool interface dynamics using a simplified mathematical formulation and three frequency response measurements on a single artifact [26]. Montevecchi et al. described inverse coupling for determining the rotational degrees of freedom without additional experiments [27]. Similarly, Fregolent showed experimentally that for a decoupling case, rotational degrees of freedom can be neglected and substituted with FRFs having translational degrees of freedom [28]. In 2017, Qi et al. [29] provided a receptance coupling analysis that included rotations using a Timoshenko beam model and showed experimental validation of the model. In the same year, Montevecchi et al. [30] used two connection points and eliminated the measurement and computation of rotational degrees of freedom in the use of RCSA to predict tool tip FRFs.

In 2018, Liao et al. [31] described an experimental technique for determining the rotational receptances from measured translational receptances using a single setup. Gibbons et al. [32] then showed instability in the use of finite differencing to determine rotational degrees of freedom when measurement spacing is small and data is non-exact. A method for selecting optimized measurement spacing based on analytical error analysis was presented. Next, Xuan et al. [33] calculated rotational receptances by finite element analysis and measured the translational receptances using modal testing. Ji et al. [34] described two compensation strategies to compute the rotational stiffness receptances with improved accuracy. In 2022, Iglesias et al. [35] provided an overview of several dynamic characterization methods and examined how each addresses effects which may or may not be captured by other methods. The paper discusses traditional methods, including impact hammer excitation, shaker excitation, and machine drive excitation, and new methods, including excitation for rotating tools, parameter extraction from cutting tests, operational modal analysis, cutting force excitation modal analysis, and digital image correlation. The relationship of these measurement methods to RCSA data collection was described.

4. Tool-holder receptance modeling

Accurate models of the tool and holder are naturally required for accurate tool tip receptance predictions. Many authors have addressed this modeling issue. In 2003, Kivanc and Budak [36] described an equivalent diameter beam for fluted endmills based on the cross-sectional moment of inertia (or second moment of area). They studied both static and dynamic models for endmills and holders. In 2004, the same authors [37] considered the relationship between fluted geometry and modeled cross-sectional properties using RCSA. They compared static and dynamic receptance predictions for carbide and high-speed steel tools to measurements. In 2006, Koplow et al. [38] derived an analytical solution for the response of a beam with a step change in diameter. The authors compared the analytical solution to experimental analysis and RCSA solutions.

In 2009, Zhongqun et al. [39] implemented a beam with two diameters that represented the tool shank and fluted section, where the equivalent diameter of the fluted section was based on the cross-sectional moment of inertia. The inertia was calculated as the sum of the inertias for each flute. Joint parameters between the tool and holder were identified by nonlinear least-squares fitting using the measured and predicted FRF. Filiz et al. [40] applied a

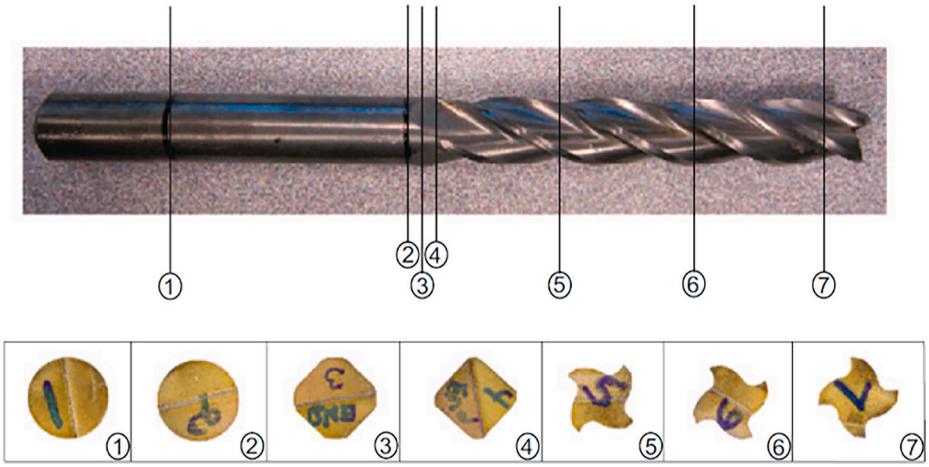

Fig. 9. Cross-sections of carbide endmill prepared using electrical discharge machining (EDM). The MATLAB image processing toolbox was used to identify the image boundary (periphery) and points were extracted to define the cross-section [43].

Table 1
Tool and holder modeling topics.

Topic	References
Euler-Bernoulli beam model	1, 2, 7-11, 102
Timoshenko beam model	14, 29, 42, 52, 56, 64, 65, 71, 94, 104, 119, 135, 150
Equivalent diameter for fluted portion	36-39, 41, 45
Spectral-Tchebychev model	40, 43

spectral-Tchebychev technique with the Timoshenko beam model to form a parameterized solution. They compared the predicted response to a finite element model of the tool-holder assembly and validated the approach experimentally. Kumar [41] described an equivalent diameter beam model for estimating the dynamics of the fluted portion of endmills to avoid computationally expensive finite element analysis in RCSA applications.

In 2011, Zhang et al. [42] presented an RCSA model for the machine-spindle-holder-tool assembly, where measured machine-spindle dynamics were coupled to Timoshenko beam models of the holder and tool shank. This result was then coupled to a finite element model of the tool's fluted portion. In 2012, Bediz et al. [43] described a model of the three-dimensional response for endmills based on a spectral-Tchebychev technique. The model considered the actual fluted geometry of the endmill and comparisons to experiments and finite element analysis models were presented for bending, axial, and torsional modes. Fig. 9 displays the sectioned geometry for a carbide endmill used in the study. In 2015, Özşahin and Altintas [44] predicted tool tip FRFs using RCSA with helix angle and lag angle considered when defining the fluted section of the endmill. They showed the variation in tool tip response with angular spindle position. In 2018, Tunc [45] implemented an STL slicing algorithm to determine the cross-sectional properties of the fluted section of the endmill and used the slices to develop an improved beam model for RCSA. Table 1 summarizes the topics and associated references for the tool-holder receptance modeling.

5. Connection modeling

The tool-holder connection stiffness and damping has received significant attention in the literature. Despite best efforts by holder manufacturers to provide a stiff interface, it cannot be considered rigid in general. The complex-valued, frequency-dependent connection stiffness matrix defined in Eq. (15) has been evaluated, and modified, by several authors. Researchers have identified a dependence of the connection parameters on holder type (e.g., thermal shrink fit vs. collet), tool diameter, and tool extension length from the holder. In addition, the spindle-holder connection stiffness and damping have also been studied for the taper interface (e.g., HSK or CAT).

In 2003, Kivanc and Budak [46] used experimental data and finite element analysis to perform static and dynamic analyses of tools with varying geometry, where RCSA was used to combine individual components. The authors evaluated effects of changes of tool parameters and clamping conditions and coupling parameters were determined through nonlinear least-squares fitting. In the same year, Schmitz and Burns [47] examined potential simplifying assumptions when predicting tool tip receptances by RCSA. Over a range of tool lengths, the authors compared the least squares fit of the coupling parameters to a logarithmic interpolation between the longest and shortest tool. Good agreement was found between the predicted and measured tool point receptances. In 2005, Agapiou [48] evaluated the stiffness of holder-spindle interfaces by impact testing and finite element analysis. Linear and rotational spring elements were compared to user-selected angular stiffness in the numerical solutions.

In 2006, Ertürk et al. [49] studied the effects of bearings and contact parameters on the resulting tool point FRF using RCSA. A comparison to finite element analysis predictions was provided. In the same year, Budak [50] used RCSA to predict the tool tip FRF using joint parameters identified by least-squares error minimization between prediction and measurement. Movahhedy and Gerami [51] applied an optimization method based on a genetic algorithm to find the spindle rotational responses from bending modes to determine the stiffness and damping parameters. In the same year, Namazi [52] presented a model for the holder-spindle interface using experimental data and finite element analysis. The author used Timoshenko elements to model CAT and HSK tapers while evaluating the effect of drawbar force on the interface dynamics.

In 2007, Ertürk et al. [53] concluded that variations in the values of rotational contact parameters do not affect the predicted FRF as strongly as translational parameters. They used average values for the rotational terms and analyzed the effects of bearing dynamics, spindle-holder interface dynamics, holder-tool interface dynamics, and bearing and interface damping values on the predicted tool tip FRF. Lee and Hwang [54] used a gradient-based optimization algorithm to identify connection parameters. They evaluated the method for noisy FRFs and found that it was able to accurately identify connection stiffnesses, while damping parameter accuracy decreased with noise level. Also in 2007, Ahmadi and Ahmadian [55] modeled the tool-holder joint as a zero thickness interface with variable stiffness. Damping in the selected

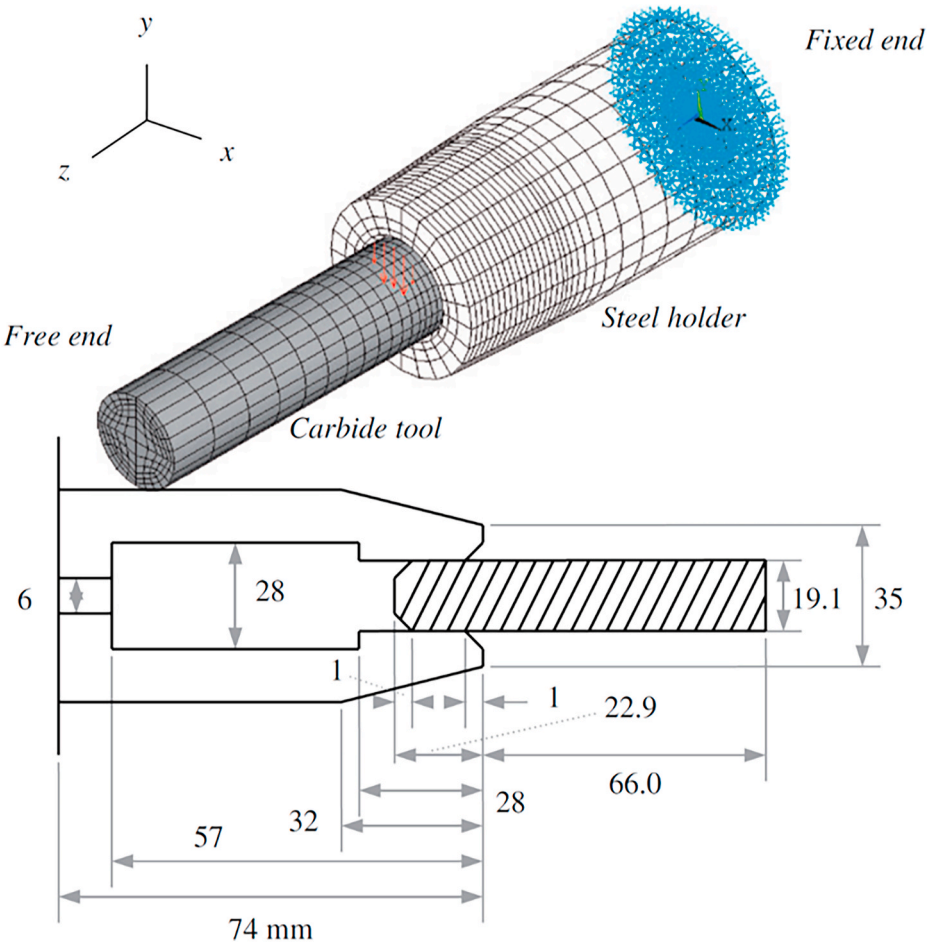

Fig. 10. Finite element model for 19.1 mm diameter carbide tool blank inserted in steel tapered shrink fit holder. The base of the holder was held fixed, while the end of the tool was unsupported [57].

model was displacement dependent. Namazi et al. [56] used uniformly distributed springs to model the holder-spindle taper contact and identify the spring constants by error minimization between experiment and model. The holder-tool was modeled by Timoshenko beam elements. The authors also modeled the influence of wear at the contact by removing springs from the holder-spindle interface. Schmitz et al. [57] used a finite element modeling approach to determine connection parameters for a shrink fit holder. Position-dependent stiffness and viscous damping values between the cutting tool and holder were used to determine the tool tip FRF by RCSA. The ANSYS finite element model is shown in Fig. 10 with 6324 20-node cubic elements (SOLID184), 768 8-node contact elements (CONTA174), and 768 8-node target elements (TARGE170) were applied, where the flexible-to-flexible contact/target elements were located at the interface between the tool and holder; this gave a total of 29467 nodes.

In 2008, Mascardelli et al. [58] used measurements of gage tools to determine spindle dynamics and coupling parameters. They then implemented RCSA to predict the dynamics and stable machining conditions for micro-endmills. Özşahin et al. [59] determined tool-holder contact parameters for a limited set of tool diameters and extensions lengths experimentally. These results were used to train a neural network for the estimation of parameters in other assembly configurations. Park and Chae [60] evaluated the dynamics of modular tooling (screw-on type milling cutters) to identify the joint parameters at the connection.

In 2009, O. Özşahin et al. [61] simplified the RCSA equations to obtain a closed-form solution for the complex stiffness matrix at the tool-holder and spindle-holder joints. They found that the solution was highly sensitive to noise due to the required matrix inversions. In 2010, Ahmadian and Nourmohammadi [62] combined a measured spindle-machine FRF with analytical tool and holder FRFs and distributed joint interfaces between the three components. The approach was used to model different tool-holder combinations assuming the same conditions at the interfaces. Rezaei et al. [63] applied inverse RCSA to extract tool-holder joint parameters. These parameters were used to predict FRFs for tools with varying extension lengths.

In 2011, Mancisidor et al. [64,65] presented the use of a fixed boundary approach and Timoshenko beam model with restrained movement to determine the free-free response of the tool. In 2012, Rezaei et al. [66] described an inverse RCSA method, where the tool-holder FRFs were determined by measurement and the analytical tool was removed from the holder response. In this method, the joint parameters were a function of the holder and did not need to be identified specifically. Ghanati and Madoliat [67] used finite element analyses to model continuous tool-holder and holder-spindle boundaries and determine coupling parameters. The authors presented a method that used the measured FRFs of the machine-spindle and the tool-holder model to predict tool tip FRFs.

In 2013, Wang et al. [68] used particle swarm optimization to identify the connection parameters between a tool and holder given artifact measurements of the spindle dynamics. Zhai et al. [69] evaluated the stiffness of the holder-spindle joint under varying drawbar forces. Mehrpouya et al. [70] compare the use of inverse RCSA and a point-mass model to identify joints in an assembled structure. The authors concluded that the two methods yielded similar results, while inverse RCSA method required fewer measurements and computation

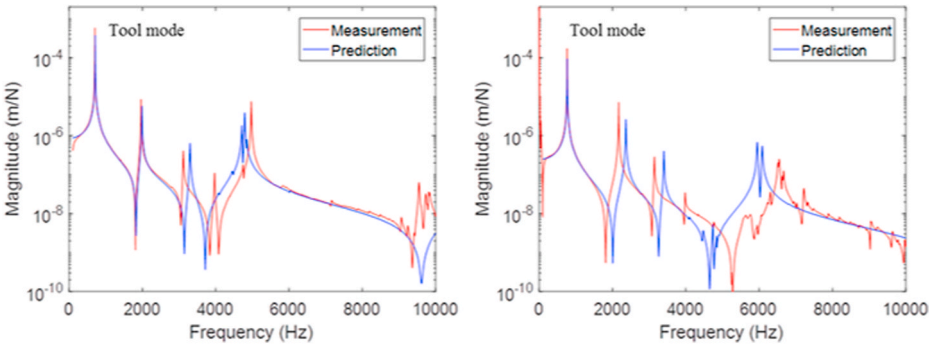

Fig. 11. Tool tip FRF predictions and measurements. (Left) 12.7 mm diameter tool with 112.70 mm length. (Right) 19.05 mm diameter tool with 113.77 mm length [87].

time. Building on their 2011 studies in 2014, Mancisidor et al. [71] presented the use of a fixed boundary approach and Timoshenko beam model with restrained movement to determine the free-free response of the tool. The authors demonstrated improved accuracy in RCSA results for slender tools versus non-standard tools. A comparison was provided between stability limits generated using FRF measurements, FRF predictions by RCSA, and cutting tests. The amplitude and frequency between measured and predicted FRFs were compared for slender and non-slender tools in three types of tool holders and three different machine spindles. Also in 2014, W. Xiao et al. [72] reported a finite element model with solid spindle and holder elements and a zero thickness, zero mass joint element containing stiffness and damping. Joint parameters were extracted from measured FRF data. The radial, tangential, and axial effects of the interface were considered. Liu et al. [73] used inverse RCSA to isolate the modal parameters of a high speed face mill from machine effects for improved dynamic design of the tool.

In 2015, Mehrpouya et al. [74] used inverse RCSA to determine the properties of joints by comparing the differences in measured versus predicted structure receptances. The application was the dynamic prediction of new structures with the same joint configuration. Grossi et al. [75] analyzed collet, shrink fit, and hydraulic tool-holder connections based on three-dimensional solid element modeling. Finite element solutions were compared to free-free boundary condition impact tests. Accuracy improvement in receptance predictions were shown for finite element analysis versus single degree of freedom beam models. Özşahin et al. [76] recognized that bearing dynamics change due to gyroscopic moments, centrifugal forces, and thermal expansion during high speed machining operations. They simultaneously employed an inverse stability solution for the chatter problem and Timoshenko beam models with RCSA as a novel and accurate method to identify bearing stiffness and damping under operational conditions. A stability diagram was presented that included the effects of gyroscopic moments and bearing stiffness variations.

In 2016, Zhu et al. [77] identified holder-tool coupling parameters by inverse RCSA; a Cuckoo search algorithm was implemented to determine the complex stiffness matrix. In the same year, Mehrpouya et al. [78] presented a six degree of freedom model for each assembly joint and include translational and rotational FRFs with consideration for the inertial properties of the joint. Matthias et al. [79] described a method to determine tool-holder contact parameters from free-free measurements. An ER32 collet connection was investigated with varying tool diameters, clamping torque, extension length, and tool material. The authors showed that multiple parameter sets are valid for a single setup, but only the parameters found via free-free measurement were capable of producing accurate predictions for different extension lengths. Yang et al. [80] predicted the tool tip FRF of a tool in a collet holder by modeling the joint interfaces of the collet-holder and collet-tool assemblies as distributed zero thickness damped-elastic layers. Yang et al. [81] also modeled the tool-holder-spindle assembly

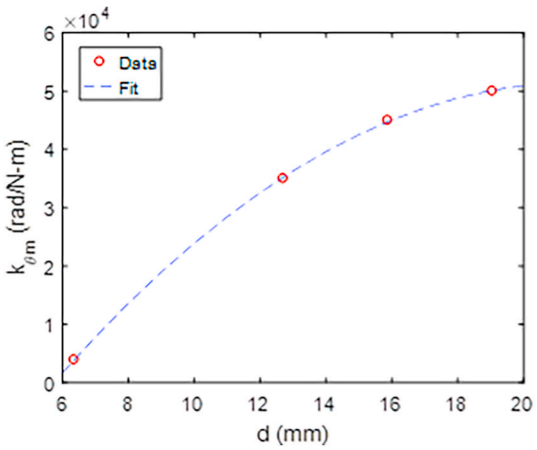

Fig. 12. Second-order variation in the rotation-to-moment stiffness with tool diameter [87].

as four substructures (spindle-holder, tool shank, tool flutes, and tool-holder interface). They modeled the tool-holder joint as a zero-thickness distributed layer with spring-damper elements.

In 2017, Liao et al. [82] described a relationship between contact stiffness and load based on Hertzian contact and fractal geometry theories. They evaluated the effects of radial interference, insertion length, and rotational speed on contact behavior for RCSA predictions. Pour and Ghorbani [83] used RCSA and a multi-objective optimization algorithm (NSGA-II) to evaluate coupling parameters based on contact length, clamping torque, and tool length-to-diameter ratio.

In 2018, Yang et al. [84] used a double joint model to account for the tool-collet and collet-holder interfaces using two sets of spring-damper elements to determine the three-dimensional dynamics for a spindle-holder-tool system. In 2019, Hung et al. [85] presented a comparison between tool tip frequency responses determined by finite element models of the entire machine tool structure to those calculated by RCSA using individual substructures to evaluate machine tool design performance. Also in 2019, Wan et al. [86] evaluated the spindle-holder contact characteristics and pressure distributions under clamping and centrifugal forces. Schmitz et al. [87] applied a 7-point coupling model between the holder and tool for four tool diameters and 16 total extension lengths. The authors showed a second-order dependence on the rotation-to-moment stiffness parameter which varied by tool diameter when all other complex stiffness matrix terms were kept constant. Fig. 11 displays tool tip FRF predictions and measurements for two tool diameters with nominally the same extension length. The variation in $k_{\theta m}$ from Eq. (15) is shown in Fig. 12; all other parameters were kept constant. The second order dependence was:

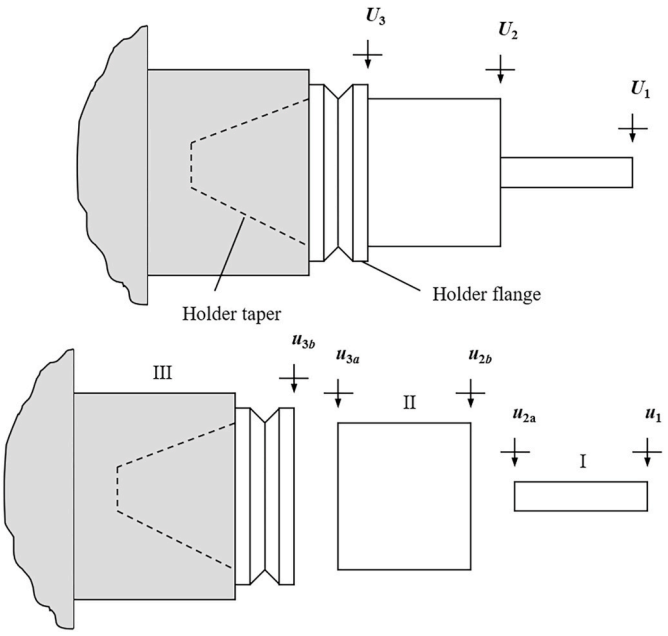

Fig. 13. Three-component RCSA model with the spindle-machine identified as component III. (Top) assembly. (Bottom) components [14].

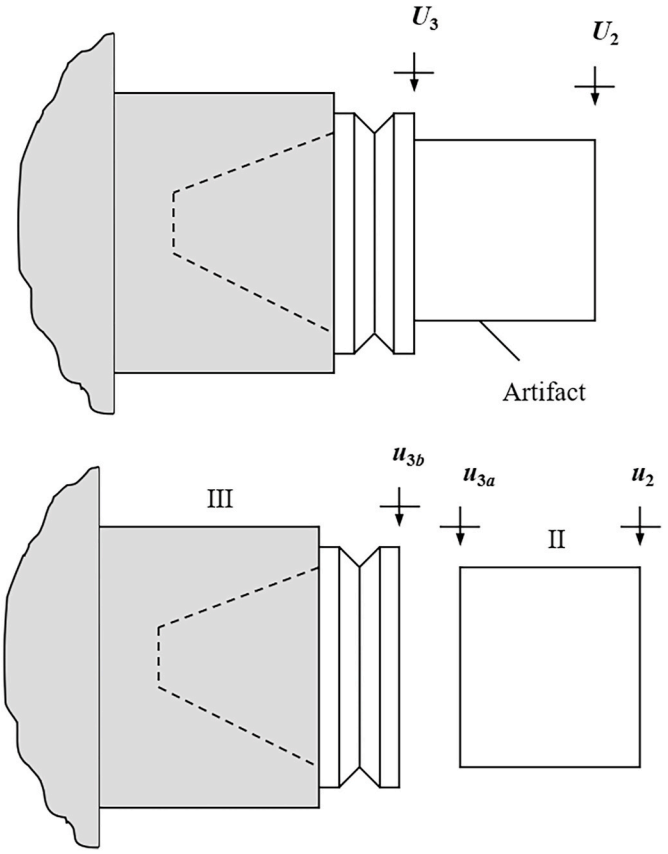

Fig. 14. Artifact-spindle-machine model. (Top) assembly. (Bottom) components [14].

$$k_{\theta m} = ad^2 + bd + c \left(\frac{\text{rad}}{\text{N}} - \text{m}\right) \tag{16}$$

where d is the tool diameter in mm, $a = -284$ (−336.2, −71.85), $b = 8824$ (5488, 12160), and $c = -43940$ (−62870, −25010). For the fitting parameters a-c, both the mean value and the 95% confidence bounds are provided.

In 2020, Čiča et al. [88] compared a genetic algorithm (GA), simulated annealing (SA), and particle swarm optimization (PSO) as soft computing methods for identifying spindle-holder-tool contact parameters. They used an adaptive neural fuzzy interference system (ANFIS) to predict holder-tool contact parameters. In 2021, Astarloa et al. [89] used RCSA to characterize the clamping conditions of a boring bar and predict the tool tip FRFs for boring bars with varying lengths. Brecher et al. [90] identified coupling parameters using a free-free approach for a heat shrink HSK-63A tool-holder combination. They used a finite element model to describe the asymmetric geometry of the interface portion of the holder. Beam models were used from the flange to tool tip. They selected an objective function to minimize the weighted difference between the frequencies of the predicted and measured resonant peaks. They modeled an effective diameter by using coupling coefficients from measurement of blanks and optimizing for diameter. In 2022, Akbari et al. [91] developed a method for modeling the contact dynamics of a tool in holder under free-free boundary conditions based on a nonlinear optimization of the sound spectrum of the impacted tool.

6. Spindle-machine receptances

As noted in Section 3, in 2005 Duncan and Schmitz [14] applied a three-component RCSA model and identified the spindle-machine receptances using a standard artifact; see Fig. 13, where the tool is component I, the holder is component II, and the spindle-machine is component III, which contains the machine, spindle, portion of the holder inside the spindle (i.e., the taper), and the holder flange. This is a convenient separation point for the holder because the flange geometry is consistent for any spindle-holder interface, such as HSK-63A or CAT-40. This is required for automatic tool changers to have a uniform geometry to grip.

As shown in Section 2, the tool (component I) and holder (II) receptances can be modeled using beam theory and the generalized receptance matrices, R_{ij}, can be populated. For the spindle-machine (III), however, measurements are necessary because the required information is not generally available to accurately model this complex component. To enable identification of both the displacement and rotation receptances, a standard artifact is inserted in the spindle. The artifact-spindle-machine model is displayed in Fig. 14. It is composed of the portion of the artifact beyond the spindle flange (component II) and the spindle-machine (component III), where the spindle-machine receptances are required to predict the tool tip receptances for arbitrary combinations of tools and holders inserted in the selected spindle-machine.

The artifact-spindle-machine receptances are written by modifying Eq. (13). By replacing coordinate 1 with 2, coordinate 2a with 3a, and coordinate 2b with 3b, the assembly receptances in Eq. (16) are obtained.

$$\boldsymbol{G_{22}} = \boldsymbol{R_{22}} - \boldsymbol{R_{23a}}(\boldsymbol{R_{3a3a}} + \boldsymbol{R_{3b3b}})^{-1}\boldsymbol{R_{3a2}} = \begin{bmatrix} H_{22} & L_{22} \\ N_{22} & P_{22} \end{bmatrix} \tag{16a}$$

unlike the tool-holder-spindle-machine model, where the desired prediction outcome is the tool tip assembly receptances contained in the generalized matrix $\boldsymbol{G_{11}}$ (Eq. (13)), the intent in this case is to determine the component receptances $\boldsymbol{R_{3b3b}}$. This generalized receptance matrix contains the receptances for the spindle-machine, which are not conveniently modeled or measured. To determine $\boldsymbol{R_{3b3b}}$, an inverse RCSA approach is applied where Eq. (16) is rewritten to solve for $\boldsymbol{R_{3b3b}}$. See Eq. (17).

$$\boldsymbol{R_{3b3b}} = \boldsymbol{R_{3a2}}(\boldsymbol{R_{22}} - \boldsymbol{G_{22}})^{-1}\boldsymbol{R_{23a}} - \boldsymbol{R_{3a3a}} = \begin{bmatrix} h_{3b3b} & l_{3b3b} \\ n_{3b3b} & p_{3b3b} \end{bmatrix} \tag{17}$$

Here, the $\boldsymbol{G_{22}}$ assembly receptances are measured, while the $\boldsymbol{R_{22}}$,

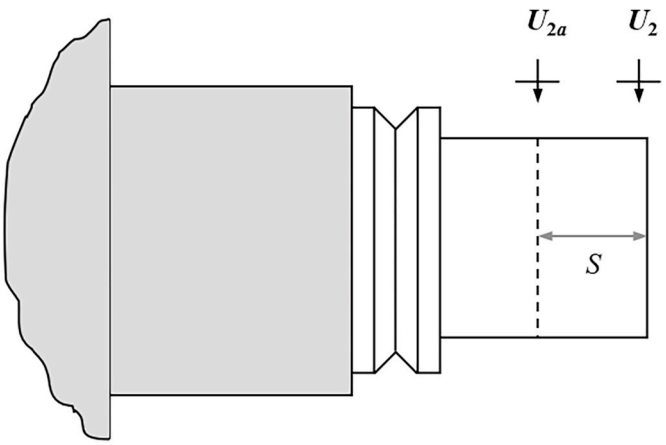

Fig. 15. Direct and cross artifact-spindle-machine assembly measurement locations used to determine assembly rotation-to-force receptance N_{22} [92].

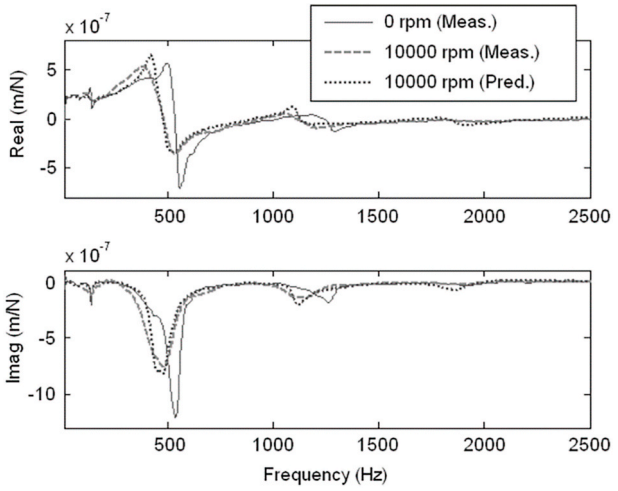

Fig. 16. Comparison of 0 rpm measurement (solid line) to 10,000 rpm measurement (dashed) and prediction (dotted) for 25.4 mm diameter tool inserted in a collet holder. A significant change in the tool point FRF with speed is observed [95].

$\boldsymbol{R_{23a}}$, $\boldsymbol{R_{3a2}}$, and $\boldsymbol{R_{3a3a}}$ component receptances are modeled. As before, either Euler-Bernoulli or Timoshenko beam models may be applied to describe the component receptances. To determine the four $\boldsymbol{G_{22}}$ receptances, the displacement-to-force direct receptance $H_{22} = \frac{X_2}{F_2}$ may be measured by tap testing, where an impact hammer is used to excite the artifact-spindle-machine assembly at coordinate 2 and the response is measured at the same location using a low-mass accelerometer or other linear sensor. To find the rotation-to-force receptance $N_{22} = \frac{\Theta_2}{F_2}$, a first-order finite difference approach may be implemented [92]. By measuring both the direct receptance H_{22} and the cross receptance $H_{2a2} = \frac{X_{2a}}{F_2}$, N_{22} may be calculated using Eq. (18). The displacement-to-force cross receptance H_{2a2} is obtained by exciting the assembly at $\boldsymbol{U_2}$ and measuring the response at coordinate $\boldsymbol{U_{2a}}$, located a distance S from the artifact's free end, as shown in Fig. 15. Equivalently, H_{22a} could be measured, where the linear transducer is placed at $\boldsymbol{U_2}$ and the force is applied at $\boldsymbol{U_{2a}}$.

$$H_{22} = \frac{H_{22} - H_{2a2}}{S} = \frac{H_{22} - H_{22a}}{S} \tag{18}$$

The other off-diagonal term in Eq. (16) $\boldsymbol{G_{22}}$ matrix term is assigned by reciprocity, $L_{22} = N_{22}$. Finally, P_{22} may be determined by synthesis using Eq. (19) [93]. Given a fully populated assembly matrix, $\boldsymbol{G_{22}}$, Eq. (17) may be used to determine the spindle-machine receptances and this result may be archived and used to predict the tool tip receptance for any tool-holder combination.

$$P_{22} = \frac{\Theta_2}{M_2} = \frac{F_2}{X_2}\frac{X_2}{M_2}\frac{\Theta_2}{F_2} = \frac{1}{H_{22}}L_{22}N_{22} = \frac{N_{22}^2}{H_{22}} \tag{19}$$

In 2006, Budak et al. [94] described an analytical method that employed Timoshenko beam theory, RCSA, and structural modification techniques to model spindle-holder-tool assemblies in machining centers to predict the tool point FRF. The method was applied to optimize the spindle geometry and bearing locations for maximum dynamic stiffness at a desired frequency or frequency range. The technique was improved chatter stability by prescribing tooling and clamping conditions. In 2007, Cheng et al. [95] measured artifact displacement-to-force receptances during rotation to capture the speed-dependent spindle dynamics. These measurements were coupled with tool-holder models to predict speed-dependent tool tip FRFs and the corresponding milling stability map. Fig. 16 shows non-rotating and at-speed FRFs measurements and predictions. It is seen that the FRF magnitudes and frequencies shift with spindle speed.

In 2010, Park and Rahnama [96] applied modal testing of a shaft in a rotating spindle to determine the variation in spindle dynamics at speed. These machine-holder dynamics were coupled with a tool model to

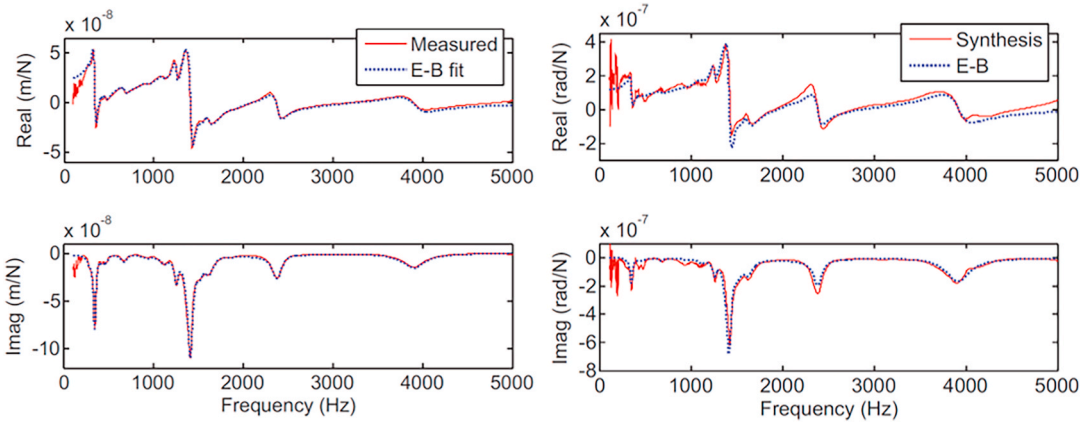

Fig. 17. Euler-Bernoulli (E-B) fixed-free beam fitting to identify rotational spindle-machine FRFs. (Left) A single measurement is performed at the free end of an artifact mounted in the spindle and each mode is fit as a fixed-free E-B beam. (Right) Comparison of rotation-to-force FRFs using the E-B approach and synthesis, where direct and cross FRFs are differenced to determine rotation. The E-B approach is able to identify the rotational FRFs using a single measurement [98,99].

predict the tool point response. In 2012, Ozturk et al. [97] used inverse RCSA to identify spindle dynamics with changing preload. Also in 2012, Kumar and Schmitz [98,99] used a single, direct FRF measurement of an artifact mounted in a spindle to identify displacement and rotational spindle-machine receptances. Each mode in the direct FRF was fit as a fixed-free beam using a close-form Euler-Bernoulli model [1]. The rotational receptances were then obtained from the same beam models. A comparison between the Euler-Bernoulli fixed-free beam fitting approach for determining rotational FRFs and the synthesis approach, where direct and cross FRFs are combined (see Eqs. (18) and (19)), is provided in Fig. 17. In 2013, Ganguly and Schmitz [100] presented the use of particle swarm optimization to fit the artifact-spindle-machine displacement-to-force modal parameters versus the prior manual fitting approaches. Fixed-free Euler-Bernoulli beams were used to model each mode in the measurement bandwidth.

In 2015, Özşahin et al. [101] addressed differences that are observed between the stability maps predicted by FRFs measured at the idle state and the actual stability behavior during machining. To identify the in-process tool point FRF, they presented a reverse solution of the chatter eigenvalue problem. Zhu et al. [102] applied the three-component RCSA approach to rotating FRF prediction by defining three substructures: the machine-spindle-holder-partial tool (inserted in the holder), the extended shank, and the fluted section of the tool. Measurements on the rotating tool shank were coupled to an Euler-Bernoulli beam model of the fluted section to predict rotating tool tip FRFs. The direct measurement of the rotating shank receptances eliminated the need to define the tool-holder coupling parameters.

In 2016, Grossi et al. [103] used cutting test results for an initial screening tool to determine speed-dependent FRFs and stability maps. Inverse RCSA was next applied to determine the speed-dependent spindle response without the tool. The rotating response for an arbitrary tool length was then determined by coupling to the rotating spindle solution. In 2017, Yan et al. [104] measured rotating spindle dynamics by impact testing on a smooth rotating tool with an accelerometer mounted on a stationary spindle head. Rotating spindle dynamics were coupled with finite element models of an actual tool using RCSA to predict the rotating tool tip FRF. In 2018, Jasiewicz and Powałka [105] used inverse RCSA to predict the spindle dynamics for a lathe and eliminated the measurements required to identify rotational degrees of freedom. Also in 2018, Li et al. [106] used experimental modal analysis to determine the machine-spindle-holder dynamics and applied RCSA to predict the tool tip FRF. Stability maps were then generated.

In 2019, Cong et al. [107] used RCSA to predict the tool tip FRF for a tool inserted in an aerostatic spindle and studied variation in spindle bearings and drawbar force conditions. RCSA coupling parameters were identified for the tool-holder and holder-shaft connections. Özşahin et al. [108] measured spindle dynamics using non-contact excitation and provided spindle speed-dependent mode shapes based on finite element analysis. Tool tip FRFs were predicted by coupling the tool model with the measured spindle dynamics.

In 2020, Ji et al. [109] used FRFs measured on the milling tool shank and an RCSA model of the fluted section to determine speed-dependent FRFs. The method provided a reduction in error due to measurement noise and uncertainty in the stability limit between a smooth rod (used in other publications) and the actual endmill. In 2021, Kim et al. [110] compared and analyzed the limitations of multiple compensation strategies to estimate rotational receptances. In 2022, Ji et al. [111] predicted rotating tool tip FRFs based on measurements of the tool shank near the holder interface. RCSA was used to predict the tool tip FRF considering a parameterized model of the fluted section of the tool.

7. Applications

Given the predictive capability afforded by RCSA, many research groups have applied it to assembly dynamics prediction in milling and other scenarios. This section lists these applications that stem from the 2000 paper [2] and subsequent method improvements.

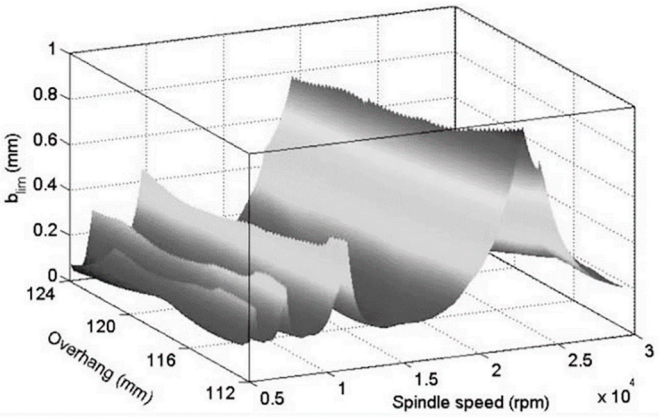

Fig. 18. Example 3-D stability surface for 12.7 mm diameter tool milling an aluminum alloy (two flutes, 100% radial immersion) [118].

In 2003, Schmitz et al. [112] described an Internet-based application to enable pre-process milling parameter selection for stable cutting conditions by RCSA. In 2004, Park and Altintas [113,114] used low-cost piezo-electric force sensors integrated into the spindle housing to measure cutting forces during milling. A Kalman filter was used to remove the effects of structural modes and reconstruct actual forces at the tool tip from the distorted forces measured by the sensors. RCSA was used to update the filter with changes in tool length. Kiefer [115] described a non-contact electromechanical actuator that was used to measure modal characteristics of a machine tool. The author used three receptances measured by the actuator to characterize the machine dynamics and predict the tool tip FRF by RCSA. Burns and Schmitz [116] demonstrated that, for certain tool extension lengths from the holder, the tool dynamics couple with the spindle dynamics and result in a dynamic absorber effect and increased dynamic stiffness. Schmitz [117] described a compensation method for correcting measurements collected using non-ideal sensor placement. By combining experimental data with modeled responses using RCSA, the response at a desired location was predicted without conducting tests at that location. This method enabled selection of high signal-to-noise ratio measurement locations. Schmitz et al. [118] expanded the traditional stability map with spindle speed and axial depth of cut to include a third dimension describing the dependence on endmill extension length. The dependence was determined analytically using RCSA for a given tool and was implemented for tool tuning applications to optimize material removal rates. An example 3-D stability surface is provided in Fig. 18, where the vertical axis is the limiting depth of cut to avoid chatter, b_{lim}.

In 2005, Cheng et al. [119] used RCSA to predict tool tip dynamics for micro-scale endmill applications. Timoshenko beams were used to model the tool and holder. Duncan et al. [120] applied RCSA to investigate the effect of interactions between modes of individual structures which, when combined, result in an increased dynamic stiffness and an associated improvement in the critical stability limit. This effect was evaluated for a stacked flexure and spindle-holder-tool assembly.

In 2006, Park [121] implemented RCSA to predict the transfer function between force experienced at the tool tip and spindle-mounted piezoelectric force sensors. The system provided force calibration for varying tool extension lengths. In 2007, Ertürk et al. [122] assessed the effects of system design and operating parameters on the tool tip FRF and chatter stability using RCSA with a Timoshenko beam model. The authors showed that it is possible to modify the stability map and maximize the chatter-free material removal rate by selecting favorable system parameters using RCSA. Dhupia et al. [123] used nonlinear RCSA to predict the tool tip FRF for a column-spindle structure. Weak nonlinearities at the joints resulted in modifications to the structural dynamics and stability behavior with force amplitude changes.

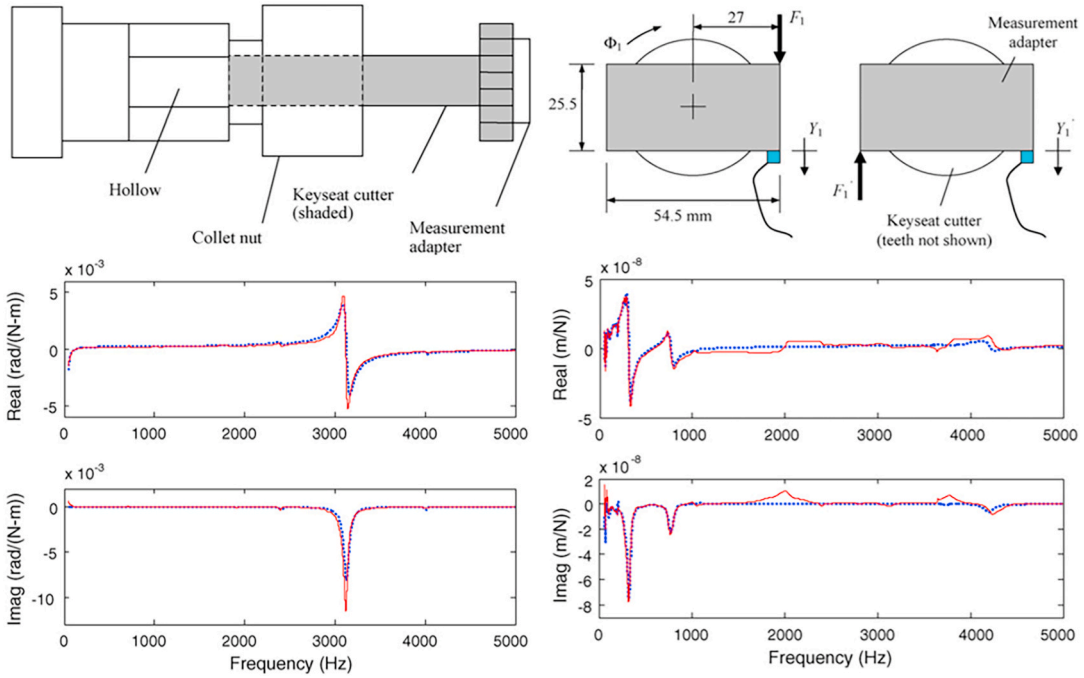

Fig. 19. Torsional and axial FRF modeling by RCSA. (Top left) Keyseat cutter model. (Top right) Measurement adapter used to measure torsional FRF. (Bottom left) Measured and predicted torsional FRFs. (Bottom right) Measured and predicted axial FRFs [128].

In 2009, Banerjee et al. [124] used RCSA and string test measurements for tools with high flexibility which can be difficult to measure by impact testing. Malekian et al. [125] developed a mechanistic force model for ploughing and shearing in micro-milling based on run-out, dynamics, and elastic recovery of the material. RCSA was implemented to determine the dynamic response since tool tip measurements were not feasible. In 2010, Malekian et al. [126] identified the shear, rotational, and axial dynamics of a bovine intervertebral disc using modal analysis and RCSA. The dynamics of discs with and without fusion were compared. In the same year, Özşahin et al. [127] presented a structural modification method using RCSA to compensate the mass effect of accelerometers during a dynamic measurement. The study showed discrepancies between accelerometers and laser vibro meters for FRF measurement of the same structure. Schmitz [128] described the use of RCSA to predict torsional and axial responses for a free-free beam. The method was applied for two tool-holder-spindle-machine assemblies. Example prediction and measurement results for a 38.7 mm outer diameter, 16-tooth high-speed steel key seat cutter clamped in a collet holder are shown in Fig. 19. Dan et al. [129] predicted the performance of a gantry-style machine design by coupling a finite element model of the machine with a tool to predict tool tip dynamics by RCSA.

In 2011, Mehrpouya, and Park [130] used RCSA to model the dynamics of an atomic force microscope (AFM) setup and probe. In 2012, Ding et al. [131] modeled spindle-workpiece dynamics using RCSA for a diamond turning application. Also in 2012, Ding et al. [132] described the use of RCSA to determine the tool tip response as an input to time domain simulation of milling. In 2013, Law et al. [133] studied position-dependent tool tip FRFs using RCSA. The tool-holder response for three different machine substructure models was presented. In 2014, Law et al. [134] used RCSA to evaluate the performance of a mobile machining system with varying boundary conditions that resulted in different connection stiffness and damping. Özşahin et al. [135] employed a Timoshenko beam model, which included the effect of gyroscopic moments, for modeling rotor segments. Sub-segment FRFs were obtained analytically and coupled using RCSA. The results indicated that the use of the Timoshenko beam model and RCSA significantly reduced

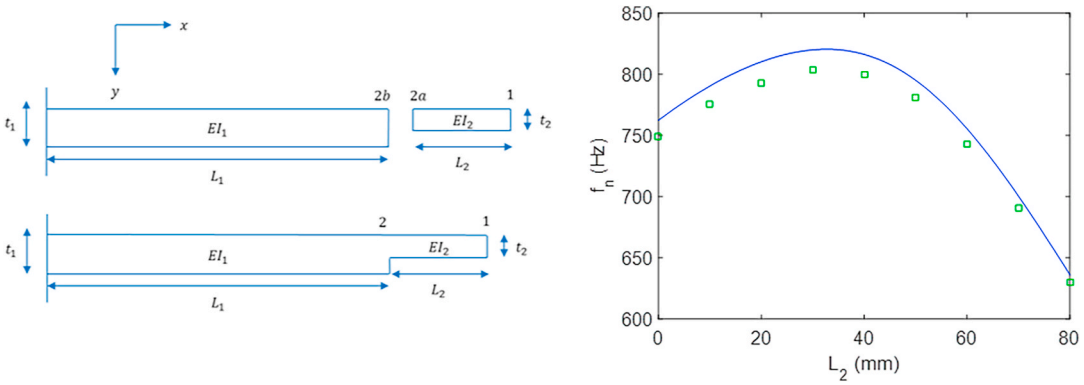

Fig. 20. Application of RCSA to thin rib machining. (Left) Beam model for RCSA where the two components and associated coordinates (1 and 2*a* for the free-free component and 2*b* for the fixed-free component) are identified (top) and the assembly and associated coordinates (1 and 2) are shown (bottom). (Right) Graphical comparison of experiments (squares) and RCSA (line) natural frequency, f_n, predictions as the rib is machined from right to left. The initial increase in natural frequency is because the mass is reducing more quickly than the stiffness [147].

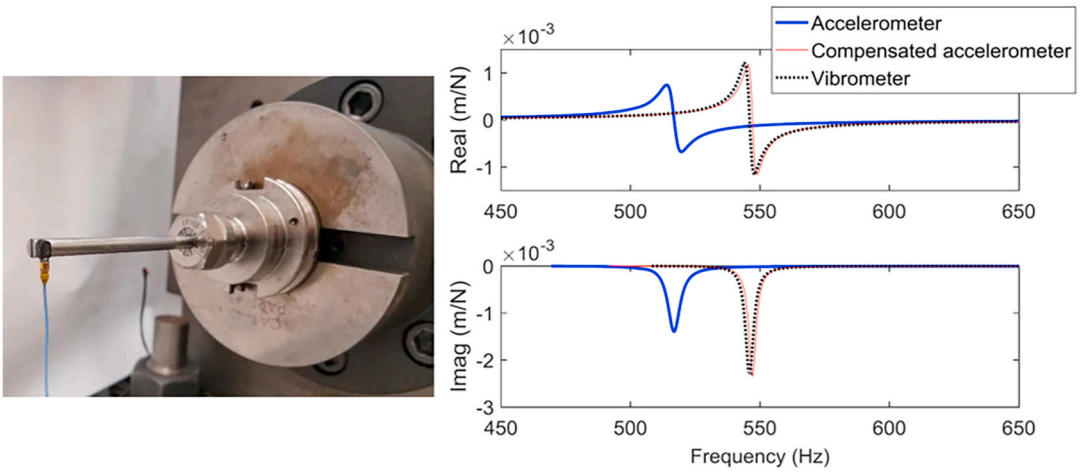

Fig. 21. Mass loading compensation for FRF measurements by RCSA. (Left) Piezoelectric accelerometer attached to the free end of a 6.35 mm diameter rod with 89 mm extension length from an ER16 collet holder using modal wax. (Right) Measured and compensated FRFs with comparison to non-contact laser vibration for validation [148,149].

computation time compared with finite element analysis without loss of accuracy. Li et al. [136] applied RCSA to a workpiece-chuck assembly to predict the FRF for a lathe workpiece. The authors evaluated the effects of various calibration shafts.

In 2015, Law and Ihlenfeldt [137] modeled the position-dependent dynamic behavior for a three-axis milling machine. Receptances at the contacting interfaces were projected to a point to facilitate a multiple-point RCSA solution. Law et al. [138] also used RCSA to predict tool point responses and state-space coupling to predict the changing nature of the plant model for mobile machines in with varying boundary conditions. Yang et al. [139] used the dynamics for all axes to predict tool tip bending, torsional, and axial receptances by RCSA. They also described a method for eliminating the effect of the adapter mass on torsional and axial receptances. Schmitz [140] evaluated the potential effects of retention knob geometry on the spindle-machine dynamics. Wang et al. [141] described a non-contact electromagnetic loading device to determine the frequency response of a spindle over a range from 0 to 12000 rpm.

In 2016, Munoa et al. [142] reviewed methods for chatter suppression in milling. RCSA was applied for tool and holder selection based on predicted dynamics and stability for a given tool length and diameter. Law et al. [143,144] presented a method for determining the free-free response of a mobile machine tool by decoupling (inverse RCSA) the mounted machine's dynamics from the dynamics of the system to which it is mounted. Jin and Koya [145] predicted the torsional-axial vibrations in drilling while including the boundary condition dynamics.

In 2017, Zhang et al. [146] determined pose-dependent spindle dynamics. They used RCSA to account for swivel motion and rotary motion at arbitrary locations from three orthogonal postures. Schmitz and Honeycutt [147] used two analytical approaches for predicting thin rib, fixed-free beam dynamics with varying geometries. The first approach applied the Rayleigh method to determine the effective mass for the fundamental bending mode of the stepped thickness beams and Castigliano's theorem to calculate the stiffness both at the beam's free end and at the change in thickness. The second method used RCSA to predict the beam receptances at the same two locations by rigidly connecting receptances that describe the individual stepped beam sections. The component receptances were derived using the Timoshenko beam model. A comparison between the RCSA predictions and experiments for thin rib machining is presented in Fig. 20.

Kiran et al. [148,149] removed the effects of mass loading and energy dissipation through cable interaction using RCSA for accelerometer-based impact testing. Fig. 21 shows the experimental setup and compensation results. This approach is particularly important for small diameter tools with low modal mass values. Xiaohong et al. [150] used RCSA to predict the tool tip FRFs for micro-endmills. A comparison was made between Timoshenko and Euler-Bernoulli beam models for the tools. Vasquez [151] described the use of structural dynamics information for pre-process parameter selection. The author proposed the integration of RCSA into computer aided manufacturing (CAM) software to enable simulation of the dynamic results in a virtual environment.

In 2018, Bansal and Law [152] implemented RCSA to tune and locate a tuned mass damper on a slender boring bar to increase the assembly's dynamic stiffness. Honeycutt and Schmitz [153] used RCSA to predict the response of a stepped beam using the Timoshenko beam model. They performed additional predictions and measurements for configurations where the stepped thickness was modified by machining. Wang et al. [154] used RCSA to predict micro-endmill tool tip FRFs; three-dimensional stability and surface location error diagrams were generated. The authors showed that stability was affected more strongly than surface location error by changes in tool length. Ealo et al. [155] used inverse RCSA to evaluate multi-body structures with several joints. They maintained calculation precision and conditioning by evaluating each joint independently. Jasiewicz and Powałka [156] predicted responses for the machine-tool-holder-workpiece dynamics for a workpiece mounted in a turning setup using measured spindle receptances and an analytical workpiece model. Junior et al. [157] implemented RCSA within a Monte Carlo simulation to identify the FRF uncertainty given uncertainty in tool length and diameter. Postel et al. [158] used FRFs collected during rotation to predict speed-dependent spindle dynamics by RCSA. Mohammadi et al. [159] described an analytical approach to modify the dynamic response of a machine tool for chatter mitigation. They predicted individual substructures and tuned them using RCSA. Their approach enabled operation-based tool diameter and length modifications to reduce chatter.

In 2019, Barrios et al. [160] used RCSA to couple a thin-walled part and robot to determine the stiffness of the assembly in a robot-assisted machining operation. Wang et al. [161] applied RCSA and transfer path analysis (TPA) to determine the tool-holder and workpiece-dynamometer contact parameters and compensate cutting forces measured by a dynamometer. Kiran and Kayacan [162] estimated changing workpiece dynamics during milling using RCSA to model the machined and unmachined areas. Inverse RCSA was used to identify the boundary condition at the clamped interface. Nagesh and Law [163] described asymmetric dynamic properties for improving the dynamic response of machine tool structures using dynamic absorber principles. Lu et al. [164] used RCSA to predict the tool tip FRF for a micro-endmill

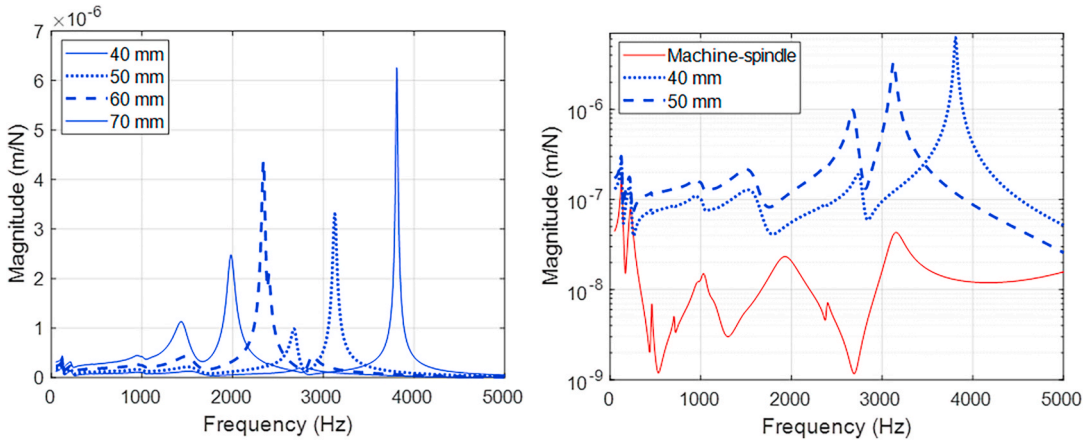

Fig. 22. Modal interactions for tool-holder-spindle-machines. (Left) Comparison of tool point FRFs for four tool extension lengths. (Right) Comparison of machine-spindle (solid line), 40 mm tool extension (dotted line), and 50 mm tool extension (dashed line) FRFs [170].

while including the centrifugal force and gyroscopic effects for high speed rotation.

In 2020, Yadav et al. [165] studied designs of integrated tuned mass dampers using analytical solutions for a damper placed at the free end of the bar. They used RCSA to identify optimal locations for the damper, which may differ from the free end of the boring bar. Chen et al. [166] applied RCSA with frequency response testing at pre-arranged postures and a standardization process to predict the tool tip FRF for an industrial milling robot at any posture. Yu et al. [167] showed that the low frequency modes of a hybrid machine tool affected the stability boundary at low speeds. They presented a dynamic model of a parallel mechanism, where RCSA of the machine-spindle-holder-tool was used to predict the tool tip FRF. In a substructure dynamics review, Su and Wang [168] discussed two methods of classical substructure synthesis, the mechanical impedance method, singular value decomposition, rigidity-flexibility equivalence, transformation of degree of freedom, reference datum method, function dynamic modification method, neural network model modification, and frequency response function modification. They described advantages and disadvantages of each method. Postel et al. [169] implemented ensemble transfer learning on deep neural networks to predict a stability boundary. Inputs to the system included a single test to determine the machine-spindle dynamics, predicted frequency response using RCSA, and guidelines about stability boundaries. Experiments were used to fine-tune the network. Schmitz [170] used RCSA to predict FRFs for a range of tool extension lengths. He demonstrated that for certain lengths, the tool-holder and machine-spindle modes interact to provide increased dynamic stiffness. He also showed the corresponding stability maps to illustrate the effects of varied dynamic stiffness. Fig. 22 (left panel) displays the tool tip FRFs for tool extensions lengths of {40, 50, 60, and 70} mm. It is observed that the 40 mm and 60 mm lengths exhibit a single, dominant vibration mode (i.e., the tool bending mode), while the 50 mm length includes two closely-space modes. The reason is interaction of a tool-holder bending mode with a spindle mode as shown in Fig. 22 (right panel). It is seen that a machine-spindle mode near 3000 Hz causes the 50 mm extension to have two dominant modes, rather than one.

Gibbons et al. [171] proposed three options for tool length tuning by RCSA: variation in holder diameter, direct structural modification for modeling the holder without knowledge of the tool-holder interface, and implementation of a tunable-mass holder. Li et al. [172] used RCSA to couple a tool-holder-shank model to a model of the fluted portion obtained from to a 3D scan of the tool. Rotational FRFs were determined by inverse RCSA. Greis et al. [173] implemented RCSA to predict tool-point FRFs for the generation of stability maps in a physics-guided machine learning framework.

In 2021, Karataş [174] offered an optimization method to suppress tool tip FRF peaks by adding a tool-holder extension subassembly and matching the dominant mode of the tool-holder extension subassembly with the effective modal frequency at the holder tip. They employed RCSA to assemble holder-spindle, holder extension, and tool receptances. The collective results demonstrated improvements in the dynamic stiffness and chatter-free material removal rate. Mostaghimi et al. [175] used RCSA to predict the dynamics between the tool tip and spindle housing. Spindle current sensors and spindle housing-mounted accelerometers were suggested as a low-cost alternative to a table top dynamometer for cutting force measurements. Shaik et al. [176] predicted tool tip dynamics using RCSA and finite element analysis of the holder-spindle interface. Constant contact stiffness and variations in structural damping were evaluated and compared to experiments. The authors used a genetic algorithm and simulated annealing methods to minimize the error between experimental and predicted responses. Bertelsen et al. [177] argued that the common practice of choosing the shortest tool may not always result in the best productivity and that local optima exist for certain extension lengths as shown by modal testing results (i.e., tool tuning). Akbari and Ahmadi [178] applied RCSA to model vibration-assisted drilling (VAD) tool holder dynamics to determine the vibration response due to piezoelectric actuation for axial and axial-torsional VAD holders. Ma et al. [179] designed a two degree of freedom, shank-mounted tuned mass damper using RCSA. The intent was tunable tool tip dynamics for a micro-endmill. Ma et al. [180] also applied RCSA to design a tool holder with a tuned mass damper to improve the stability limit for an extended reach endmill. Danylchenko et al. [181] implemented RCSA to determine tool-workpiece interactions.

In 2022, Bilgili et al. [182] present a method for modeling multi-axis machine tool dynamics with pose changes using Jacobian-based kinematics. The method was found to be 90% faster than existing models. Morelli et al. [183] used RCSA to predict the tool-holder-spindle-machine FRFs along the tool axis. These FRFs are used together with the milling force model to predict surface location error in 2.5-axis peripheral milling operations. Kato et al. [184] used RCSA to analyze a carbon fiber reinforced plastic (CFRP) spindle shaft design. A motorized CFRP spindle unit was modeled by combining a spindle shaft model and bearing models. Wu et al. [185] combined RCSA with experimental modal analysis to obtain a dynamic model of the TriMule robot. They used the model to predict the milling stability behavior over the entire robot workspace. Ji et al. [186] applied inverse RCSA to model the variation in tool tip FRF prediction caused by the mass of multiple accelerometers on a setup.

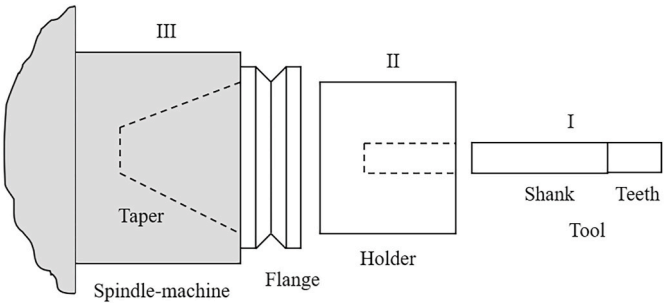

Fig. 23. RCSA components for future research efforts.

8. Conclusions and future research

This paper provided a review of publications that implement and advance the receptance coupling substructure analysis (RCSA) approach first applied to tool tip receptance (frequency response function) prediction for milling applications in 2000 [2]. The review topics include tool-holder receptance modeling (section 4), connection modeling (section 5), spindle-machine receptances (section 6), and applications (section 7). In total, 178 papers were identified that have collectively received 7113 citations (Google Scholar, March 2022).

While significant research and implementation progress has been made, knowledge gaps remain. These gaps are summarized with respect to Fig. 23 in the following paragraphs, where the relevant component (I, II, or III) or component combination (e.g., I-II) is specified, as well as the paper section.

- (I, section 4) Tool modeling has made significant progress, including representing the helical teeth in beam models, but a comprehensive, computationally-efficient solution that is generic to common, but complex tool geometries (e.g., solid carbide endmills with serrated edges and indexable endmills with many inserts) has not be made widely available. Structured light scanning may provide a route forward to develop and distribute a tool model database, e.g., Refs. [187–191]. Leadership from cutting tool manufacturers would enhance this effort.
- (II, section 4) Similar to tools, holder modeling has received attention in the literature. Remaining obstacles include accurate geometric information about internal geometries and specialized clamping strategies, such as hydraulic holders. The latter have received less attention in the literature. A coordinated effort from holder manufacturers to release solid models with internal features and dimensions would add value to the RCSA approach.
- (I-II, section 5) The connection modeling between the tool and holder has been examined in many studies. However, a unified model does not yet exist. Some models artificially place the flexibility and damping (e.g., lumped parameter linear spring and viscous damper) at the location where the base of the tool shank meets the face of the holder. Others distribute the flexibility and damping at the actual contact interface between the tool shank outer diameter and holder internal cylindrical cavity. It's been observed that the connection parameters vary with shank diameter, which is to be expected since the contact area varies with diameter. However, sensitivity to tool extension length (beyond the holder face) has also been reported. A complete, first principles model for the tool-holder connection would greatly benefit the RCSA approach.
- (III, section 6) Several methods have been demonstrated to measure and represent the linear and rotational spindle-machine receptances under both non-rotating and rotating conditions. Given the complexity of spindles and the supporting machine tool structure, a measurement-free solution with sufficient accuracy may be difficult (or impossible) to obtain. However, removing the measurement requirement entirely would expand the opportunities to apply RCSA for tool tip receptance prediction.
- (II-III, section 5) Quantifying and modeling the stiffness and damping at the holder-spindle taper interface has received less attention in the literature. In most cases, the connection is included in the spindle-machine receptances rather than modeled separately. Additional research is warranted.
- (I-II-III, section 7) The significant interest in machine learning and its application to machining process modeling and optimization pose a significant opportunity for RCSA, e.g., Refs. [192–198]. Because the tool tip receptance is a key input to milling performance prediction and it varies with each unique tool-holder-spindle-machine combination, RCSA will be an essential element of these machine learning scenarios if generalized solutions are to be obtained.
- (I-II-III, section 7) As the digital twin for machining is universally implemented, predictive models will be incorporated to describe the system dynamics. Data about the tool tip receptances will naturally be included, so RCSA models provide an important capability.

Declaration of competing interest

The authors declare that they have no known competing financial interests or personal relationships that could have appeared to influence the work reported in this paper.

Acknowledgements

This work was supported by the DOE Office of Energy Efficiency and Renewable Energy (EERE), Advanced Manufacturing Office (AMO), under contract DE-AC05-00OR22725. The US government retains and the publisher, by accepting the article for publication, acknowledges that the US government retains a nonexclusive, paid-up, irrevocable, worldwide license to publish or reproduce the published form of this manuscript, or allow others to do so, for US government purposes. DOE will provide public access to these results of federally sponsored research in accordance with the DOE Public Access Plan (http://energy.gov/downloads/doe-public-access-plan).

References

[1] Bishop RED, Johnson DC. The mechanics of vibration. Cambridge, UK: Cambridge University Press; 1960.
[2] Schmitz TL, Donaldson RR. Predicting high-speed machining dynamics by substructure analysis. CIRP Annals 2000;49(1):303–8.
[3] Altintas Y, Budak E. Analytical prediction of stability lobes in milling. CIRP Annals 1995;44(1):357–62.
[4] Altintas Y, Stepan G, Budak E, Schmitz T, Kilic ZM. Chatter stability of machining operations. J Manuf Sci Eng 2020;142(11).
[5] Altintas Y. Manufacturing automation: metal cutting mechanics, machine tool vibrations, and CNC design. Cambridge, UK: Cambridge University Press; 2000.
[6] Schmitz T, Smith S. Machining dynamics: frequency response to improved productivity. second ed., vol. 2019. New York, NY: Springer; 2009.
[7] Schmitz T, Smith KS. Mechanical vibrations: modeling and measurement. second ed., vol. 2020. New York, NY: Springer; 2012.
[8] Weaver Jr W, Timoshenko S, Young D. Vibration problems in engineering. fifth ed. New York, NY: John Wiley and Sons; 1990.
[9] Schmitz T, Davies M, Kennedy M. High-speed machining frequency response prediction for process optimization. In: Proceedings of the 2nd international seminar on improving machine tool performance, La Baule, France; 2000, July. p. 3–5.
[10] Schmitz TL, Davies MA, Medicus K, Snyder J. Improving high-speed machining material removal rates by rapid dynamic analysis. CIRP Annals 2001;50(1):263–8.
[11] Schmitz TL, Davies MA, Kennedy MD. Tool point frequency response prediction for high-speed machining by RCSA. J Manuf Sci Eng 2001;123(4):700–7.
[12] Park SS, Altintas Y, Movahhedy M. Receptance coupling for end mills. Int J Mach Tool Manufact 2003;43(9):889–96.
[13] Burns TJ, Schmitz TL. A study of linear joint and tool models in spindle-holder-tool receptance coupling. In: International design engineering technical conferences and computers and information in engineering conference, vol. 47438; 2005, January. p. 947–54.
[14] Schmitz TL, Duncan GS. Three-component receptance coupling substructure analysis for tool point dynamics prediction, vol. 127; 2005. p. 781–90. 4.

[15] Duncan GS, Schmitz T. An improved RCSA model for tool point frequency response prediction. In: Proceedings of the 23rd International Modal Analysis Conference. 30; 2005, January.
[16] Duncan GS. Milling dynamics prediction and uncertainty analysis using receptance coupling substructure analysis. Dissertation, University of Florida; 2006.
[17] Schmitz T, Smith KS. Machining dynamics: frequency response to improved productivity. New York, NY: Springer; 2009.
[18] Schmitz T, Smith KS. Mechanical vibrations: modeling and measurement. New York, NY: Springer; 2012.
[19] Schmitz T, Dutterer B. Machine tool genome Project case study. In: American society for precision engineering Annual meeting; 2012. October 21-October 26, San Diego, CA.
[20] Schmitz T. Machine Tool Genome Project: tool point dynamics prediction for improved milling productivity. In: Proceedings of international conference on advances in production and industrial engineering 2015, February. India: Tamil Nadu; 2015. p. 20–1.
[21] Schmitz TL, Duncan GS. Receptance coupling for dynamics prediction of assemblies with coincident neutral axes. J Sound Vib 2006;289(4–5):1045–65.
[22] Albertelli P, Goletti M, Monno M. A new receptance coupling substructure analysis methodology to improve chatter free cutting conditions prediction. Int J Mach Tool Manufact 2013;72:16–24.
[23] Albertelli P, Goletti M, Monno M. An improved receptance coupling substructure analysis to predict chatter free high speed cutting conditions. Procedia CIRP 2013;12:19–24.
[24] Wen KL, Qi HJ. Predicting tool point FRF by RCSA in high speed milling. In: Advanced materials research, vol. 1006. Trans Tech Publications Ltd; 2014. p. 398–402.
[25] Hu T, Sun M, Yin G. An improved RCSA for identifying the spindle-holder taper joint dynamics. J Vibroeng 2014;16(7):3302–16.
[26] Brecher C, Chavan P, Fey M, Daniels M. A modal parameter approach for receptance coupling of tools. MM Sci J 2016;2016:1032–4.
[27] Montevecchi F, Grossi N, Scippa A, Campatelli G. Improved RCSA technique for efficient tool-tip dynamics prediction. Precis Eng 2016;44:152–62.
[28] Fregolent A. Substructure decoupling without using rotational DoFs: fact or fiction? Mech Syst Signal Process 2016;72:499–512.
[29] Qi B, Sun Y, Li Z. Tool point frequency response function prediction using RCSA based on Timoshenko beam model. Int J Adv Manuf Technol 2017;92(5): 2787–99.
[30] Montevecchi F, Grossi N, Scippa A, Campatelli G. Two-points-based receptance coupling method for tool-tip dynamics prediction. Mach Sci Technol 2017;21(1): 136–56.
[31] Liao J, Yu D, Zhang J, Feng P, Wu Z. An efficient experimental approach to identify tool point FRF by improved receptance coupling technique. Int J Adv Manuf Technol 2018;94(1):1451–60.
[32] Gibbons TJ, Öztürk E, Sims ND. Rotational degree-of-freedom synthesis: an optimised finite difference method for non-exact data. J Sound Vib 2018;412: 207–21.
[33] Xuan XJ, Haung ZH, Wu KD, Hung JP. Prediction of the frequency response function of a tool holder-tool assembly based on receptance coupling method. Eng Technol Appl Sci Res 2018;8(6):3555–60.
[34] Ji Y, Bi Q, Zhang S, Wang Y. A new receptance coupling substructure analysis methodology to predict tool tip dynamics. Int J Mach Tool Manufact 2018;126: 18–26.
[35] Iglesias A, Tunç LT, Özsahin O, Franco O, Munoa J, Budak E. Alternative experimental methods for machine tool dynamics identification: a review. Mech Syst Signal Process 2022;170:108837.
[36] Kivanc EB, Budak E. Modeling statics and dynamics of milling system components. In: Proceedings of 36th CIRP international seminar on manufacturing systems; 2003. p. 433–40.
[37] Kivanc EB, Budak E. Structural modeling of end mills for form error and stability analysis. Int J Mach Tool Manufact 2004;44(11):1151–61.
[38] Koplow MA, Bhattacharyya A, Mann BP. Closed form solutions for the dynamic response of Euler-Bernoulli beams with step changes in cross section. J Sound Vib 2006;295(1–2):214–25.
[39] Zhongqun L, Shuo L, Yizhuang C. Receptance coupling for end mill using 2-section step beam vibration model. In: 2009 second international conference on intelligent computation technology and automation, vol. 2. IEEE; 2009, October. p. 160–3.
[40] Filiz S, Cheng CH, Powell KB, Schmitz TL, Ozdoganlar OB. An improved tool–holder model for RCSA tool-point frequency response prediction. Precis Eng 2009;33(1):26–36.
[41] Kumar UV. Comparison of equivalent diameter end mill models for dynamics prediction by receptance coupling substructure analysis. Thesis, University of Florida; 2009.
[42] Zhang J, Schmitz T, Zhao W, Lu B. Receptance coupling for tool point dynamics prediction on machine tools. Chinese J Mechan Eng English Edition 2011;24(3): 340.
[43] Bediz B, Kumar U, Schmitz TL, Ozdoganlar OB. Modeling and experimentation for three-dimensional dynamics of endmills. Int J Mach Tool Manufact 2012;53(1): 39–50.
[44] Özşahin O, Altintas Y. Prediction of frequency response function (FRF) of asymmetric tools from the analytical coupling of spindle and beam models of holder and tool. Int J Mach Tool Manufact 2015;92:31–40.
[45] Tunc LT. Prediction of tool tip dynamics for generalized milling cutters using the 3D model of the tool body. Int J Adv Manuf Technol 2018;95(5):1891–909.
[46] Kivanc EB, Budak E. Development of analytical endmill deflection and dynamics models. In: ASME international mechanical engineering congress and exposition, vol. 37203; 2003, January. p. 85–94.
[47] Schmitz T, Burns T. Receptance coupling for high-speed machining dynamics prediction. In: Proceedings of the 21st international modal analysis conference, vol. 36; 2003, February.
[48] Agapiou JS. A methodology to measure joint stiffness parameters for toolholder-spindle interfaces. J Manuf Syst 2005;24(1):13–20.
[49] Ertürk A, Özgüven HN, Budak E. Analytical modeling of spindle–tool dynamics on machine tools using Timoshenko beam model and receptance coupling for the prediction of tool point FRF. Int J Mach Tool Manufact 2006;46(15):1901–12.
[50] Budak E. Analytical models for high performance milling. Part II: process dynamics and stability. Int J Mach Tool Manufact 2006;46(12–13):1489–99.
[51] Movahhedy MR, Gerami JM. Prediction of spindle dynamics in milling by sub-structure coupling. Int J Mach Tool Manufact 2006;46(3–4):243–51.
[52] Namazi M. Mechanics and dynamics of the tool holder-spindle interface. Doctoral dissertation. University of British Columbia; 2006.
[53] Ertürk A, Özgüven HN, Budak E. Effect analysis of bearing and interface dynamics on tool point FRF for chatter stability in machine tools by using a new analytical model for spindle–tool assemblies. Int J Mach Tool Manufact 2007;47(1):23–32.
[54] Lee DH, Hwang WS. An identification method for joint structural parameters using an FRF-based substructuring method and an optimization technique. J Mech Sci Technol 2007;21(12):2011–22.
[55] Ahmadi K, Ahmadian H. Modelling machine tool dynamics using a distributed parameter tool–holder joint interface. Int J Mach Tool Manufact 2007;47(12–13): 1916–28.
[56] Namazi M, Altintas Y, Abe T, Rajapakse N. Modeling and identification of tool holder-spindle interface dynamics. Int J Mach Tool Manufact 2007;47(9): 1333–41.
[57] Schmitz TL, Powell K, Won D, Duncan GS, Sawyer WG, Ziegert JC. Shrink fit tool holder connection stiffness/damping modeling for frequency response prediction in milling. Int J Mach Tool Manufact 2007;47(9):1368–80.
[58] Mascardelli BA, Park SS, Freiheit T. Substructure coupling of microend mills to aid in the suppression of chatter. J Manuf Sci Eng 2008;130(1).
[59] Özşahin O, Budak E, Özgüven HN. Estimation of dynamic contact parameters for machine tool spindle-holder-tool assemblies using artificial neural networks. In: Proceedings of the 3rd international conference on manufacturing engineering (ICMEN); 2008, November. p. 131–44.
[60] Park SS, Chae J. Joint identification of modular tools using a novel receptance coupling method. Int J Adv Manuf Technol 2008;35(11):1251–62.
[61] Özşahin O, Ertürk A, Özgüven HN, Budak E. A closed-form approach for identification of dynamical contact parameters in spindle-holder-tool assemblies. Int J Mach Tool Manufact 2009;49(1):25–35.
[62] Ahmadian H, Nourmohammadi M. Tool point dynamics prediction by a three-component model utilizing distributed joint interfaces. Int J Mach Tool Manufact 2010;50(11):998–1005.
[63] Rezaei MM, Movahhedy MR, Ahmadian MT, Moradi H. Development of inverse receptance coupling method for prediction of milling dynamics. In: Engineering systems design and analysis, vol. 49194; 2010, January. p. 339–46.
[64] Mancisidor I, Zatarain M, Munoa J, Dombovari Z. Fixed boundaries receptance coupling substructure analysis for tool point dynamics prediction. In: Advanced materials research, vol. 223. Trans Tech Publications Ltd; 2011. p. 622–31.
[65] Mancisidor I, Zatarain M, Munoa J, Dombovari Z. Receptance coupling for tool point dynamics prediction. In: 17th CIRP international conference on modelling of machining operations; 2011, May.
[66] Rezaei MM, Movahhedy MR, Moradi H, Ahmadian MT. Extending the inverse receptance coupling method for prediction of tool-holder joint dynamics in milling. J Manuf Process 2012;14(3):199–207.
[67] Ghanati MF, Madoliat R. New continuous dynamic coupling for three component modeling of tool-holder-spindle structure of machine tools with modified effected tool damping. ASME J Manuf Sci Eng 2012;134(2):021015.
[68] Wang E, Wu B, Hu Y, Yang S, Cheng Y. Dynamic parameter identification of tool-spindle interface based on RCSA and particle swarm optimization. Shock Vib 2013;20(1):69–78.
[69] Zhai LJ, Song XL, Cai LG. Identification of toolholder-spindle joint based on receptance coupling substructure analysis. In: Applied mechanics and materials, vol. 345. Trans Tech Publications Ltd; 2013. p. 539–42.
[70] Mehrpouya M, Graham E, Park SS. FRF based joint dynamics modeling and identification. Mech Syst Signal Process 2013;39(1–2):265–79.
[71] Mancisidor I, Urkiola A, Barcena R, Munoa J, Dombovari Z, Zatarain M. Receptance coupling for tool point dynamic prediction by fixed boundaries approach. Int J Mach Tool Manufact 2014;78:18–29.
[72] Xiao W, Mao K, Zhu M, Li B, Lei S, Pan X. Modelling the spindle-holder taper joint in machine tools: a tapered zero-thickness finite element method. J Sound Vib 2014;333(22):5836–50.
[73] Liu LN, Shi ZY, Liu ZQ, Song H. Modal analysis of high-speed face milling system based on composite structure system analysis method. In: Materials science forum, vol. 800. Trans Tech Publications Ltd; 2014. p. 408–13.
[74] Mehrpouya M, Graham E, Park SS. Identification of multiple joint dynamics using the inverse receptance coupling method. J Vib Control 2015;21(16):3431–49.
[75] Grossi N, Montevecchi F, Scippa A, Campatelli G. 3D finite element modeling of holder-tool assembly for stability prediction in milling. Procedia CIRP 2015;31: 527–32.
[76] Özşahin O, Budak E, Özgüven HN. Identification of bearing dynamics under operational conditions for chatter stability prediction in high speed machining operations. Precis Eng 2015;42:53–65.

[77] Zhu J, He D, Tian F, Zhao Q. A new prediction method of tool point frequency response function for milling cutters. China Mech Eng 2016;27(20):2765.
[78] Mehrpouya M, Sanati M, Park SS. Identification of joint dynamics in 3D structures through the inverse receptance coupling method. Int J Mech Sci 2016;105:135–45.
[79] Matthias W, Özşahin O, Altintas Y, Denkena B. Receptance coupling based algorithm for the identification of contact parameters at holder-tool interface. CIRP J Manufactur Sci Technol 2016;13:37–45.
[80] Yang Y, Wan M, Ma YC, Zhang WH. An improved method for tool point dynamics analysis using a bi-distributed joint interface model. Int J Mech Sci 2016;105:239–52.
[81] Yang Y, Yuan H, Wan M, Zhang W. Tool point analysis for bending, torsional and axial receptances of tool-holder-spindle assembly. Procedia CIRP 2016;56:233–6.
[82] Liao J, Zhang J, Feng P, Yu D, Wu Z. Identification of contact stiffness of shrink-fit tool-holder joint based on fractal theory. Int J Adv Manuf Technol 2017;90(5):2173–84.
[83] Pour M, Ghorbani H. Improving FEM model of low immersion milling process using multi-objective optimization of tool elastic support dynamic properties. Int J Adv Manuf Technol 2017;92(5):2279–97.
[84] Yang Y, Wan M, Ma YC, Zhang WH. A new method using double distributed joint interface model for three-dimensional dynamics prediction of spindle-holder-tool system. Int J Adv Manuf Technol 2018;95(5):2729–45.
[85] Hung JP, Wu KD, Lin WZ, Shih WC. Analyzing the dynamic characteristics of milling tool using finite element method and receptance coupling method. Eng Technol Appl Sci Res 2019;9(2):3918–23.
[86] Wan S, Hong J, Du F, Fang B, Li X. Modelling and characteristic investigation of spindle-holder assembly under clamping and centrifugal forces. J Mech Sci Technol 2019;33(5):2397–405.
[87] Schmitz T, Honeycutt A, Gomez M, Stokes M, Betters E. Multi-point coupling for tool point receptance prediction. J Manuf Process 2019;43:2–11.
[88] Čiča Đ, Zeljković M, Tešić S. Dynamical contact parameter identification of spindle-holder-tool assemblies using soft computing techniques. Facta Univ – Ser Mech Eng 2020;18(4):565–77.
[89] Astarloa A, Fernandes MH, Mancisidor I, Munoa J, Dombovari Z. Prediction of the dynamic stiffness of boring bars. In: IOP conference series: materials science and engineering, vol. 1193. IOP Publishing; 2021, October, 012007. No. 1.
[90] Brecher C, Chavan P, Fey M. Efficient joint identification and fluted segment modelling of shrink-fit tool assemblies by updating extended tool models. J Inst Eng Prod 2021;15(1):21–33.
[91] Akbari VOA, Postel M, Kuffa M, Wegener K. Improving stability predictions in milling by incorporation of toolholder sound emissions. CIRP J Manufactur Sci Technol 2022;37:359–69.
[92] Sattinger SS. Method for experimentally determining rotational mobilities of structures. Shock Vibrat Bulletin(United States) 1980:50.
[93] Ewins DJ. Modal testing: theory, practice and application. John Wiley & Sons; 2009.
[94] Budak E, Ertürk A, Özgüven HN. A modeling approach for analysis and improvement of spindle-holder-tool assembly dynamics. CIRP Ann 2006;55(1):369–72.
[95] Cheng CH, Schmitz TL, Duncan GS. Rotating tool point frequency response prediction using RCSA. Mach Sci Technol 2007;11(3):433–46.
[96] Park SS, Rahnama R. Robust chatter stability in micro-milling operations. CIRP Annals 2010;59(1):391–4.
[97] Ozturk E, Kumar U, Turner S, Schmitz T. Investigation of spindle bearing preload on dynamics and stability limit in milling. CIRP Annals 2012;61(1):343–6.
[98] Kumar UV, Schmitz TL. Spindle dynamics identification for receptance coupling substructure analysis. Precis Eng 2012;36(3):435–43.
[99] Kumar UV. Improved spindle dynamics identification technique for receptance coupling substructure analysis. Dissertation, University of Florida; 2012.
[100] Ganguly V, Schmitz TL. Spindle dynamics identification using particle swarm optimization. J Manuf Process 2013;15(4):444–51.
[101] Özşahin O, Budak E, Özgüven HN. In-process tool point FRF identification under operational conditions using inverse stability solution. Int J Mach Tool Manufact 2015;89:64–73.
[102] Zhu J, Wang J, Zhang T, Li X. An improved tool point frequency response function prediction method based on RCSA. China Mech Eng 2015;26(3):285.
[103] Grossi N, Sallese L, Montevecchi F, Scippa A, Campatelli G. Speed-varying machine tool dynamics identification through chatter detection and receptance coupling. Procedia CIRP 2016;55:77–82.
[104] Yan R, Tang X, Peng F, Li Y, Li H. RCSA-based method for tool frequency response function identification under operational conditions without using noncontact sensor. J Manuf Sci Eng 2017;139(6).
[105] Jasiewicz M, Powałka B. Identification of a lathe spindle dynamics using extended inverse receptance coupling. J Dyn Syst Meas Control 2018;140(12).
[106] Li Z, Wang Z, Shi X, Li W. RCSA-based prediction of chatter stability for milling process with large axial depth of cut. Int J Adv Manuf Technol 2018;96(1):833–43.
[107] Cong DC, Hwang J, Shim J, Ro SK, Schmitz T. Effects of a drawbar design and force on multipurpose aerostatic spindle dynamics. Int J Mach Tool Manufact 2019;144:103424.
[108] Özşahin O, Ritou M, Budak E, Rabréau C, Le Loch S. Identification of spindle dynamics by receptance coupling for non-contact excitation system. Procedia CIRP 2019;82:273–8.
[109] Ji Y, Bi Q, Yu L, Ren F, Wang Y. A robust RCSA-based method for the in situ measurement of rotating tool-tip frequency response functions. J Manuf Sci Eng 2020;142(8):081004.
[110] Kim JW, Lee JW, Kim KW, Kang JH, Yang MS, Kim DY, Lee SY, Jang JS. Estimation of the frequency response function of the rotational degree of freedom. Appl Sci 2021;11(18):8527.
[111] Ji Y, Dong H, Yu L, Ren F, Bi Q, Wang Y. Determining rotating tool-tip FRFs by measuring holder-point FRFs based on a robust frequency-based substructure method. Mech Syst Signal Process 2022;164:108228.
[112] Schmitz TL, Tummond M, Duncan GS, Zahner C, Snyder JP. Development of an Internet-based platform for high-speed milling process parameter selection. In: Proceedings of the 18th Annual American society for precision engineering meeting, Portland, Oregon, October 26-31; 2003.
[113] Park SS, Altintas Y. Dynamic compensation of spindle integrated force sensors with Kalman filter. J Dyn Syst Meas Control 2004;126(3):443–52.
[114] Altintas Y, Park SS. Dynamic compensation of spindle-integrated force sensors. CIRP Annals 2004;53(1):305–8.
[115] Kiefer AJ. Integrating electromechanical actuator hardware with receptance coupling substructure analysis for chatter prediction on high speed machining centers. Thesis: North Carolina State University; 2004.
[116] Burns TJ, Schmitz TL. Receptance coupling study of tool-length dependent dynamic absorber effect. In: ASME international mechanical engineering congress and exposition, vol. 47136; 2004, January. p. 993–1000.
[117] Schmitz TL. Improved sensor data utility through receptance coupling modeling. In: ASME international mechanical engineering congress and exposition, vol. 47055; 2004, January. p. 411–7.
[118] Schmitz TL, Burns TJ, Ziegert JC, Dutterer B, Winfough WR. Tool length-dependent stability surfaces. Mach Sci Technol 2004;8(3):377–97.
[119] Cheng CH, Schmitz TL, Arakere N, Duncan GS. An approach for micro end mill frequency response predictions. In: ASME international mechanical engineering congress and exposition, vol. 42231; 2005, January. p. 1139–45.
[120] Duncan GS, Tummond MF, Schmitz TL. An investigation of the dynamic absorber effect in high-speed machining. Int J Mach Tool Manufact 2005;45(4–5):497–507.
[121] Park SS. Identification of spindle integrated force sensor's transfer function for modular end mills. J Manuf Sci Eng 2006;128(1):146–53.
[122] Ertürk A, Budak E, Özgüven HN. Selection of design and operational parameters in spindle–holder–tool assemblies for maximum chatter stability by using a new analytical model. Int J Mach Tool Manufact 2007;47(9):1401–9.
[123] Dhupia JS, Powalka B, Ulsoy AG, Katz R. Effect of a nonlinear joint on the dynamic performance of a machine tool. ASME J Manuf Sci Eng 2007;129(5):943–50.
[124] Banerjee A, Bordatchev EV, Feng HY. Determination of minimum limiting axial depth of cut for 2½D pocket machining based on receptance coupling. Mach Sci Technol 2009;13(2):177–95.
[125] Malekian M, Park SS, Jun MB. Modeling of dynamic micro-milling cutting forces. Int J Mach Tool Manufact 2009;49(7–8):586–98.
[126] Malekian M, Trieu D, Owoc JS, Park SS, Hunter CJ. Investigation of the intervertebral disc and fused joint dynamics through experimental modal analysis and the receptance coupling method. J Biomech Eng 2010;132(4):041004.
[127] Özşahin O, Özgüven HN, Budak E. Analysis and compensation of mass loading effect of accelerometers on tool point FRF measurements for chatter stability predictions. Int J Mach Tool Manufact 2010;50(6):585–9.
[128] Schmitz TL. Torsional and axial frequency response prediction by RCSA. Precis Eng 2010;34(2):345–56.
[129] Dan X, Rui K, Qiang L. Research on NC machine tool dynamic characteristic considering processing dynamics. In: 2010 international conference on intelligent system design and engineering application, vol. 2. IEEE; 2010, October. p. 227–31.
[130] Mehrpouya M, Park SS. Prediction of atomic force microscope probe dynamics through the receptance coupling method. Rev Sci Instrum 2011;82(12):125001.
[131] Ding Y, Li L, Krause A, Riemer O. Frequency response prediction of spindle-workpiece assemblies for ultra-precision diamond turning based on substructure analysis. In: Proc. of the 12th euspen international conference, stockholm Sweden; 2012. P4.
[132] Ding H, Ding Y, Zhu L. On time-domain methods for milling stability analysis. Chin Sci Bull 2012;57(33):4336–45.
[133] Law M, Altintas Y, Phani AS. Rapid evaluation and optimization of machine tools with position-dependent stability. Int J Mach Tool Manufact 2013;68:81–90.
[134] Law M, Rentzsch H, Ihlenfeldt S. Evaluating mobile machine tool dynamics by substructure synthesis. In: Advanced materials research, vol. 1018. Trans Tech Publications Ltd; 2014. p. 373–80.
[135] Özşahin O, Özgüven HN, Budak E. Analytical modeling of asymmetric multi-segment rotor-bearing systems with Timoshenko beam model including gyroscopic moments. Comput Struct 2014;144:119–26.
[136] Li H, Xue G, Zhou Y, Li H, Wen B. Receptance coupling for frequency response prediction of cylindrical workpiece in CNC lathe. J Vibroeng 2015;17(4):1731–47.
[137] Law M, Ihlenfeldt S. A frequency-based substructuring approach to efficiently model position-dependent dynamics in machine tools. Proc Inst Mech Eng - Part K J Multi-body Dyn 2015;229(3):304–17.
[138] Law M, Rentzsch H, Ihlenfeldt S. Development of a dynamic substructuring framework to facilitate in situ machining solutions using mobile machine tools. Procedia Manuf 2015;1:756–67.
[139] Yang Y, Zhang WH, Ma YC, Wan M. Generalized method for the analysis of bending, torsional and axial receptances of tool–holder–spindle assembly. Int J Mach Tool Manufact 2015;99:48–67.
[140] Schmitz TL. Investigation of retention knob geometry on machining dynamics. Procedia Manuf 2015;1:578–83.

[141] Wang X, Guo Y, Chen T. Measurement research of motorized spindle dynamic stiffness under high speed rotating. Shock Vib 2015;2015.
[142] Munoa J, Beudaert X, Dombovari Z, Altintas Y, Budak E, Brecher C, Stepan G. Chatter suppression techniques in metal cutting. CIRP Annals 2016;65(2):785–808.
[143] Law M, Rentzsch H, Ihlenfeldt S, Putz M. Application of substructure decoupling techniques to predict mobile machine tool dynamics: numerical investigations. Procedia CIRP 2016;46:537–40.
[144] Law M, Rentzsch H, Ihlenfeldt S. Predicting mobile machine tool dynamics by experimental dynamic substructuring. Int J Mach Tool Manufact 2016;108:127–34.
[145] Jin X, Koya NG. Prediction of coupled torsional-axial vibrations of drilling tool with clamping boundary conditions. CIRP J Manufactur Sci Technol 2016;13:24–36.
[146] Zhang J, Li J, Xie Z, Du C, Gui L, Zhao W. Rapid dynamics prediction of tool point for bi-rotary head five-axis machine tool. Precis Eng 2017;48:203–15.
[147] Schmitz TL, Honeycutt A. Analytical solutions for fixed-free beam dynamics in thin rib machining. J Manuf Process 2017;30:41–50.
[148] Kiran K, Satyanarayana H, Schmitz T. Compensation of frequency response function measurements by inverse RCSA. Int J Mach Tool Manufact 2017;121:96–100.
[149] Satyanarayana H. Compensation of frequency response function measurements by inverse RCSA. Thesis, University of North Carolina at Charlotte; 2017.
[150] Xiaohong L, Zhenyuan J, Haixing Z, Shengqian L, Yixuan F, Liang SY. Tool point frequency response prediction for micromilling by receptance coupling substructure analysis. J Manuf Sci Eng 2017;139(7).
[151] Vasquez RE. On the use of structural dynamics in virtual manufacturing. Int J Interact Des Manuf 2017;11(1):103–14.
[152] Bansal A, Law M. A receptance coupling approach to optimally tune and place absorbers on boring bars for chatter suppression. Procedia CIRP 2018;77:167–70.
[153] Honeycutt A, Schmitz T. Receptance coupling model for variable dynamics in fixed-free thin rib machining. Procedia Manuf 2018;26:173–80.
[154] Wang D, Wang X, Liu Z, Gao P, Ji Y, Löser M, Ihlenfeldt S. Surface location error prediction and stability analysis of micro-milling with variation of tool overhang length. Int J Adv Manuf Technol 2018;99(1):919–36.
[155] Ealo JA, Garitaonandia I, Fernandes MH, Hernandez-Vazquez JM, Muñoa J. A practical study of joints in three-dimensional Inverse Receptance Coupling Substructure Analysis method in a horizontal milling machine. Int J Mach Tool Manufact 2018;128:41–51.
[156] Jasiewicz M, Powałka B. Prediction of turning stability using receptance coupling. In: AIP conference proceedings, vol. 1922. AIP Publishing LLC; 2018, January, 100005. No. 1.
[157] Junior MV, Baptista EA, Araki L, Smith S, Schmitz T. The role of tool presetting in milling stability uncertainty. Procedia Manuf 2018;26:164–72.
[158] Postel M, Özsahin O, Altintas Y. High speed tooltip FRF predictions of arbitrary tool-holder combinations based on operational spindle identification. Int J Mach Tool Manufact 2018;129:48–60.
[159] Mohammadi Y, Azvar M, Budak E. Suppressing vibration modes of spindle-holder-tool assembly through FRF modification for enhanced chatter stability. CIRP Annals 2018;67(1):397–400.
[160] Barrios A, Mata S, Fernandez A, Munoa J, Sun C, Ozturk E. Frequency response prediction for robot assisted machining. MM Sci J 2019;2019:3099–106. 04.
[161] Wang C, Qiao B, Zhang X, Cao H, Chen X. TPA and RCSA based frequency response function modelling for cutting forces compensation. J Sound Vib 2019;456:272–88.
[162] Kiran K, Kayacan MC. Effect of material removal on workpiece dynamics in milling: modeling and measurement. Precis Eng 2019;60:506–19.
[163] Nagesh S, Law M. Machine tool design with preferentially asymmetrical structures to improve dynamics and productivity. Procedia CIRP 2019;79:592–5.
[164] Lu X, Jia Z, Liu S, Yang K, Feng Y, Liang SY. Chatter stability of micro-milling by considering the centrifugal force and gyroscopic effect of the spindle. J Manuf Sci Eng 2019;141(11):111003.
[165] Yadav A, Talaviya D, Bansal A, Law M. Design of chatter-resistant damped boring bars using a receptance coupling approach. J Manufactur Mater Proc 2020;4(2):53.
[166] Chen C, Peng F, Yan R, Tang X, Li Y, Fan Z. Rapid prediction of posture-dependent FRF of the tool tip in robotic milling. Robot Comput Integrated Manuf 2020;64:101906.
[167] Yu G, Wang L, Wu J, Gao Y. Milling stability prediction of a hybrid machine tool considering low-frequency dynamic characteristics. Mech Syst Signal Process 2020;135:106364.
[168] Su J, Wang B. Research progress of synthesis and modification methods based on dynamic substructures. Shock Vib 2020;2020.
[169] Postel M, Bugdayci B, Wegener K. Ensemble transfer learning for refining stability predictions in milling using experimental stability states. Int J Adv Manuf Technol 2020;107(9):4123–39.
[170] Schmitz T. Modal interactions for spindle, holders, and tools. Procedia Manuf 2020;48:457–65.
[171] Gibbons TJ, Ozturk E, Xu L, Sims ND. Chatter avoidance via structural modification of tool-holder geometry. Int J Mach Tool Manufact 2020;150:103514.
[172] Li X, Zhu J, Tian F, Huang Z. An improved rapid prediction method of the milling tool point frequency response function. Int J Adv Manuf Technol 2020;110(3):841–52.
[173] Greis N, Nogueira M, Bhattacharya S, Schmitz T. Physics-guided machine learning for self-aware machining. In: AIAA spring symposium series, March 23-24, 2020, Palo Alto, CA; 2020.
[174] Karataş G, Özşahin O, Özgüven HN, Budak E. Design optimization of tool holder extension for enhanced chatter stability by using component mode tuning method. Procedia CIRP 2021;101:294–7.
[175] Mostaghimi H, Park CI, Kang G, Park SS, Lee DY. Reconstruction of cutting forces through fusion of accelerometer and spindle current signals. J Manuf Process 2021;68:990–1003.
[176] Shaik JH, Srinivas J, T Rao S, Rama Kotaiah K, Raghu Kumar B. Identification of practical spindle-tool interface parameters using an optimization based statistical approach. Sādhanā 2021;46(2):1–15.
[177] Bertelsen N, Alphinas R, Ørskov K. A tool tuning approximation method: exploration of the system dynamics and its impact on milling stability when amending tool stick out. In: ESAFORM 2021, 24th international conference on material forming, Liège, Belgique; 2021.
[178] Ostad Ali Akbari V, Ahmadi K. Substructure analysis of vibration-assisted drilling systems. Int J Adv Manuf Technol 2021;113(9):2833–48.
[179] Ma W, Yang Y, Jin X. Chatter suppression in micro-milling using shank-mounted Two-DOF tuned mass damper. Precis Eng 2021;72:144–57.
[180] Ma W, Yu J, Yang Y, Wang Y. Optimization and tuning of passive tuned mass damper embedded in milling tool for chatter mitigation. J Manufactur Mater Proc 2020;5(1):2.
[181] Danylchenko Y, Petryshyn A, Repinskyi S, Bandura V, Kalimoldayev M, Gromaszek K, Imanbek B. Dynamic characteristics of "tool-workpiece" elastic system in the low stiffness parts milling process. In: Mechatronic systems 2: applications in material handling processes and robotics. Routledge; 2021. p. 225–36.
[182] Bilgili D, Budak E, Altintas Y. Multibody dynamic modeling of five-axis machine tools with improved efficiency. Mech Syst Signal Process 2022;171:108945.
[183] Morelli L, Grossi N, Campatelli G, Scippa A. Surface location error prediction in 2.5-axis peripheral milling considering tool dynamic stiffness variation. Precis Eng 2022;76:95–109.
[184] Kato M, Kono D, Kakinuma Y. Dynamical characteristic validation of motorized CFRP spindle unit based on receptance coupling. Mech Syst Signal Process 2022;173:109028.
[185] Wu L, Wang G, Liu H, Huang T. An improved algorithm to predict the pose-dependent cutting stability in robot milling. Int J Adv Manuf Technol 2022:1–13.
[186] Ji Y, Chen Y, Zhang S, Bi Q, Wang Y. Multi-point substructure coupling method to compensate multi-accelerometer masses in measuring rotation-related frequency response functions. J Manuf Sci Eng 2022;144(1).
[187] No T, Gomez M, Copenhaver R, Uribe Perez J, Tyler C, Schmitz T. Force and stability modeling for non-standard edge geometry endmills. J Manuf Sci Eng 2019;141(12):121002.
[188] No T, Gomez M, Copenhaver R, Uribe Perez J, Tyler C, Schmitz T. Scanning and modeling for non-standard edge geometry endmills. Procedia Manuf 2019;34:305–15.
[189] Gomez M, No T, Smith S, Schmitz T. Cutting force and stability prediction for inserted cutters. Procedia Manuf 2020;48:443–51.
[190] Gomez M, No T, Schmitz T. Digital force prediction for milling. Procedia Manuf 2020;48:873–81.
[191] No T, Gomez M, Karandikar J, Heigel J, Copenhaver R, Schmitz T. Contributions of scanning metrology uncertainty to milling force prediction. Procedia Manuf 2021;53:213–22.
[192] Oleaga I, Pardo C, Zulaika JJ, Bustillo A. A machine-learning based solution for chatter prediction in heavy-duty milling machines. Measurement 2018;128:34–44.
[193] Karandikar J, Honeycutt A, Schmitz T, Smith S. Stability boundary and optimal operating parameter identification in milling using Bayesian learning. J Manuf Process 2020;56:1252–62.
[194] Denkena B, Bergmann B, Reimer S. Analysis of different machine learning algorithms to learn stability lobe diagrams. Procedia CIRP 2020;88:282–7.
[195] Postel M, Bugdayci B, Wegener K. Ensemble transfer learning for refining stability predictions in milling using experimental stability states. Int J Adv Manuf Technol 2020;107(9):4123–39.
[196] Greis NP, Nogueira ML, Bhattacharya S, Schmitz T. Physics-guided machine learning for self-aware machining. In: 2020 AAAI spring symposium on AI and manufacturing. Stanford University; 2020.
[197] Cornelius A, Karandikar J, Gomez M, Schmitz T. A Bayesian framework for milling stability prediction and reverse parameter identification. Procedia Manuf 2021;53:760–72.
[198] Chen G, Li Y, Liu X, Yang B. Physics-informed Bayesian inference for milling stability analysis. Int J Mach Tool Manufact 2021;167:103767.